Cell Genomics

Article

Genome-wide CRISPR screening of chondrocyte maturation newly implicates genes in skeletal growth and height-associated GWAS loci

Graphical abstract

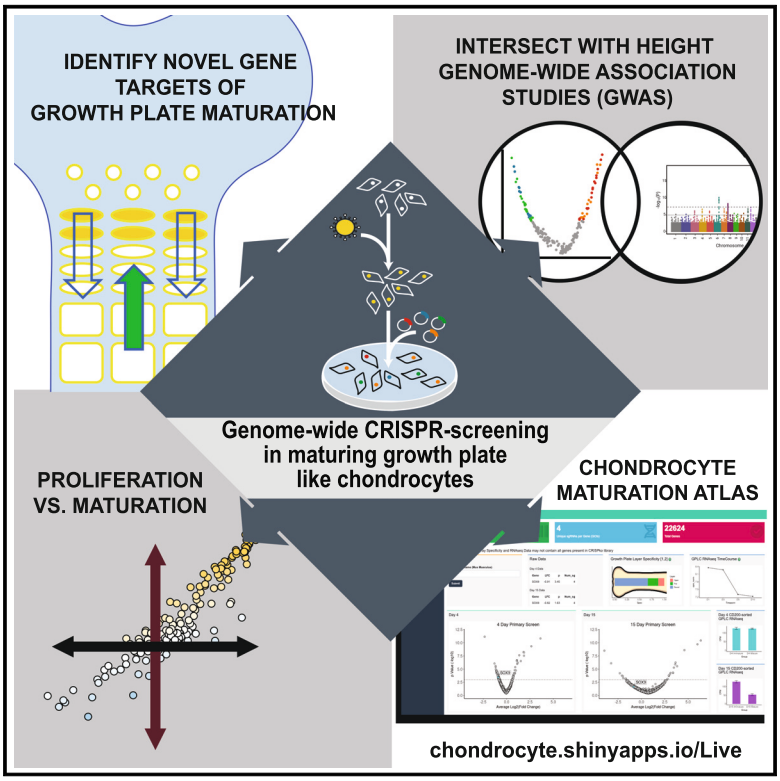

Highlights

- Genome-wide CRISPR KO study links growth-plate maturation to height GWASs
- Identified 145 genes affecting chondrocyte proliferation and maturation
- Screening targets independently predict enrichment of GWAS height heritability
- Method could be used to improve existing GWAS gene assignment algorithms

Authors

John M. Baronas, Eric Bartell, Anders Eliasen, ..., Henry M. Kronenberg, Joel N. Hirschhorn, Nora E. Renthal

Correspondence

nora.renthal@childrens.harvard.edu

In brief

Baronas et al. paired human height GWASs with functional genome-wide screening of growth-plate chondrocytes. Targets were enriched in height heritability and genes critical for endochondral ossification. This study emphasizes that functional assays in relevant tissues can refine likely causal genes from GWASs and implicates new regulators of chondrocyte maturation.

Baronas et al., 2023, Cell Genomics *3*, 100299
May 10, 2023
https://doi.org/10.1016/j.xgen.2023.100299

CellPress

Cell Genomics

CellPress
OPEN ACCESS

Article

Genome-wide CRISPR screening of chondrocyte maturation newly implicates genes in skeletal growth and height-associated GWAS loci

John M. Baronas,[1] Eric Bartell,[1,2,3] Anders Eliasen,[1,2,4,5] John G. Doench,[6] Loic Yengo,[7] Sailaja Vedantam,[1,2] Eirini Marouli,[8] GIANT Consortium, Henry M. Kronenberg,[9] Joel N. Hirschhorn,[1,2] and Nora E. Renthal[1,10,*]

[1]Department of Pediatrics, Division of Endocrinology, Boston Children's Hospital and Harvard Medical School, Boston, MA, USA
[2]Medical and Population Genetics, Broad Institute of MIT and Harvard, Cambridge, MA, USA
[3]Department of Genetics, Harvard Medical School, Boston, MA, USA
[4]COPSAC, Copenhagen Prospective Studies on Asthma in Childhood, Herlev and Gentofte Hospital, University of Copenhagen, Copenhagen, Denmark
[5]Department of Health Technology, Section for Bioinformatics, Technical University of Denmark, Kgs. Lyngby, Denmark
[6]Genetic Perturbation Platform, Broad Institute of MIT and Harvard, Cambridge, MA, USA
[7]Institute for Molecular Bioscience, The University of Queensland, Brisbane, QLD, Australia
[8]William Harvey Research Institute, Barts and the London School of Medicine and Dentistry, Queen Mary University of London, London, UK
[9]Endocrine Unit, Massachusetts General Hospital and Harvard Medical School, Boston, MA 02114, USA
[10]Lead contact
*Correspondence: nora.renthal@childrens.harvard.edu
https://doi.org/10.1016/j.xgen.2023.100299

SUMMARY

Alterations in the growth and maturation of chondrocytes can lead to variation in human height, including monogenic disorders of skeletal growth. We aimed to identify genes and pathways relevant to human growth by pairing human height genome-wide association studies (GWASs) with genome-wide knockout (KO) screens of growth-plate chondrocyte proliferation and maturation *in vitro*. We identified 145 genes that alter chondrocyte proliferation and maturation at early and/or late time points in culture, with 90% of genes validating in secondary screening. These genes are enriched in monogenic growth disorder genes and in KEGG pathways critical for skeletal growth and endochondral ossification. Further, common variants near these genes capture height heritability independent of genes computationally prioritized from GWASs. Our study emphasizes the value of functional studies in biologically relevant tissues as orthogonal datasets to refine likely causal genes from GWASs and implicates new genetic regulators of chondrocyte proliferation and maturation.

INTRODUCTION

A classical polygenic phenotype, height, is the result of childhood skeletal growth. Genome-wide association studies (GWASs) of height have identified thousands of height-associated loci in over 5 million individuals.[1–4] These loci are enriched for genes that underlie disorders of skeletal growth, members of biological pathways important for skeletal growth, and genes expressed in human and murine growth-plate chondrocytes.[1,2,5,6] Growth-plate chondrocytes elongate bone by proliferating and maturing to hypertrophy. Proper regulation of chondrocyte maturation is important, as dysregulated proliferation or hypertrophy leads to altered bone growth, with clinical consequences from short stature or overgrowth (often mild) to skeletal dysplasia (often severe).

Despite the contributions of height GWASs to our understanding of the genetics of skeletal growth, several challenges persist in translating genetic associations to biological mechanisms. Linkage disequilibrium (LD) and the fact that most GWAS variants (>80%) reside in non-coding regions,[7] with no universally accepted approach to assign SNPs to relevant genes, mean that it is difficult to identify the causal genes mediating associations seen in GWASs. Computational methods, including those that rely on locus-based and similarity-based prediction prioritization strategies, have sought to meet this need. Approaches such as DEPICT (data-driven expression-prioritized integration for complex traits),[8] MAGMA (multi-marker analysis of genomic annotation),[9] and PoPS (polygenic priority score)[10] integrate large expression, chromatin, or other datasets to identify genes and pathways shared or enriched among GWAS loci. These approaches help prioritize causal genes and work better when combined.[11] However, the large datasets on which these methods rely do not necessarily include the specific tissues most relevant to a particular trait of interest. Thus, relevant functional studies could complement computational gene prioritization methods. For functional studies to provide useful information, however, it is crucial to demonstrate their relevance to the *in vivo* phenotype, either by showing that they preferentially

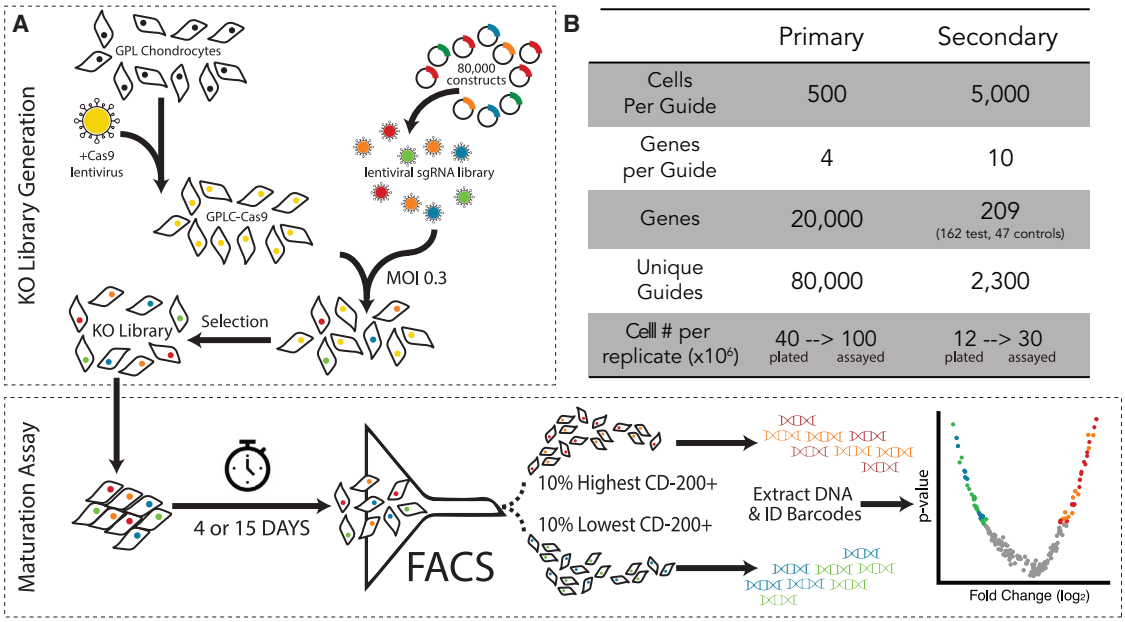

B

	Primary	Secondary
Cells Per Guide	500	5,000
Genes per Guide	4	10
Genes	20,000	209 (162 test, 47 controls)
Unique Guides	80,000	2,300
Cell # per replicate (x10^6)	40 --> 100 plated assayed	12 --> 30 plated assayed

Figure 1. Experimental overview of primary and secondary genome-wide CRISPR-Cas9 KO library screening

(A) Primary and secondary screens were conducted via identical workflows.

(B) For secondary screening, 162 genes were selected based on their significance on the primary screen, along with 47 control genes expressed in GPLCs but with no effect on primary screening. FACS, fluorescence-activated cell sorting.

identify known genes or by showing that genes or variants highlighted by functional studies are enriched for heritability in GWAS data.

Functional information from cell types of relevance may pinpoint genes not revealed by existing prioritization methods that rely on data generated from less relevant cell types; further, perturbational gene knockout (KO) data may provide information not captured by gene expression or other omics data from wild-type cells or tissues. We sought to test this hypothesis and to discover novel genes directing chondrocyte maturation by developing and implementing a functional genome-wide KO screen of chondrocyte proliferation and maturation. Our perturbational assay independently identifies known and novel genes implicated in growth-plate biology. Variants near genes implicated by our screen capture heritability from recent GWASs of human height, suggesting our findings are relevant to human skeletal growth and could be useful in refining SNP-to-gene assignment algorithms. These data provide a rich resource of gene-specific functional regulation of chondrocyte proliferation and maturation by all genes in the murine genome (available at chondrocyte.shinyapps.io/Live).

RESULTS

Genome-wide maturation screens reveal both known and novel genes and pathways in chondrocyte proliferation and maturation

We employed genome-wide CRISPR KO screening libraries[12,13] and an established *in vitro* model of the growth plate[5] to identify novel genes and pathways directing proliferation and maturation of growth-plate chondrocytes. Grown in monolayer culture, the murine cell line of growth-plate-like chondrocytes (GPLCs) expresses gene markers that mirror the maturation of the murine growth plate *in vivo* (Figure S1A), including the cell-surface chondrocyte maturation marker *CD-200*,[5,14,15] permitting high-throughput assessment of maturation by flow cytometry.[16] Having transduced GPLCs to express Cas9 and verified its robust activity (Figure S1B), we performed pooled screening using a genome-wide guide library[12] to identify genes that, when perturbed, delay or accelerate chondrocyte maturation. We selected two time points, days 4 and 15, to best probe populations of KO GPLCs maturing faster or slower than expected. Established to have low CD-200 expression (Figure S1C), we selected day 4 as a time when early maturing/CD-200-high KOs might be best observed above background. Conversely, at day 15, GLPCs exhibit high CD-200 expression (Figure S1C), permitting resolution of KO populations failing to mature given adequate time. At each time point, we collected cells with the 10% highest and 10% lowest expression of CD-200 (Figures 1 and S1D). As a control for chondrocyte maturation during screening, control GPLCs were grown in parallel under identical conditions and profiled for gene expression to affirm expected maturational markers (Figure S1A). Six-hundred million KO GPLCs were assayed for functional changes in maturation (300 million per time point), collected in replicate batches of 100 million cells, with high reproducibility for genes affecting maturation across batches (Figure S2).

We observed 140 KOs affecting GPLC maturation with $p < 0.001$ (hypergeometric distribution analysis): 97 at day 4,

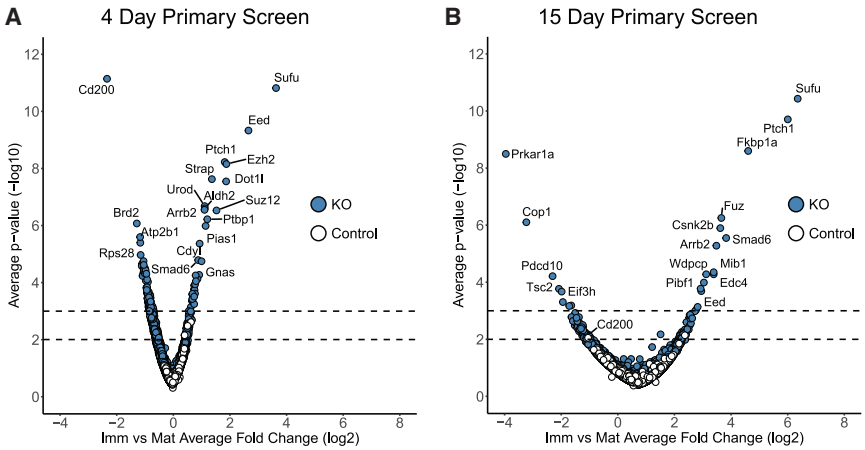

C

KEGG Pathway	Genes	Strength	FDR
Wnt signaling	Gsk3b, Bambi, Csnk2b, Lrp6, Lgr4, Apc, Ctbp1, Chd8, Trp53	0.89	0.0016
Hedgehog signaling	Ptch1, Gsk3b, Smurf2, Arrb2, Sufu	1.15	0.0101
Ubiquitin mediated proteolysis	Det1, Nedd4, Vhl, Rfwd2, Smurf2, Pias1, Prpf19	0.83	0.0144
TGF-beta signaling	Bambi, Bmpr1a, Smad6, Bmpr2, Acvr1, Smurf2	0.94	0.0144
Hippo signaling	Bbc3, Gsk3b, Bmpr1a, Yap1, Ywhae, Apc, Bmpr2	0.79	0.0144

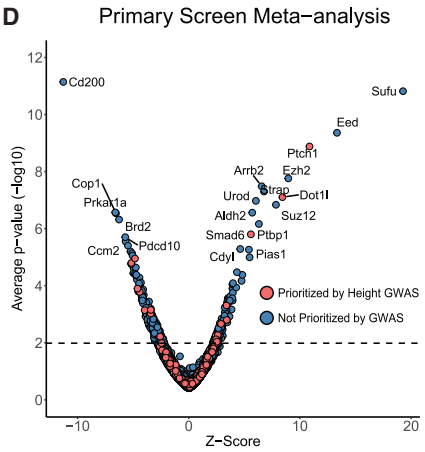

Figure 2. Genome-wide maturation screens reveal genes and pathways in chondrocyte proliferation and maturation

(A) Volcano plot of KOs from 4-day maturation screening, demonstrating average log2 fold change (LFC) between mature (top 10% CD-200-high cells) and immature (bottom 10% CD-200-low) KO populations across three replicate day 4 screens (Imm vs. Mat Average Fold Change [$\log_2$]), plotted against statistical significance (Average p value [$-\log_{10}$]). Gene KOs are shown in blue and non-targeting controls in white. Dashed lines mark $-\log_{10}p = 3$ and $-\log_{10}p = 2$ (total n_{cells} = 300 million).

(B) Volcano plot of KOs from the 15-day maturation screen, with data averaged from three replicate 15-day screens (total n_{cells} = 300 million).

(C) KEGG pathway analysis of most significant KOs on genome-wide screening.

(D) Meta-analysis of all six genome-wide screens. Genes prioritized by PoPS, MAGMA, and DEPICT from height GWAS[3] are shown in red.

30 at day 15, and 13 at both time points with a log2 fold change (LFC) > 0.57 (mature) or < −0.63 (immature). Of the KOs affecting chondrocyte maturation after 4 days, 71% (78/110) resulted in immature GPLCs and 29% (32/110) resulted in mature GPLCs (Figure 2A; Table 1). Conversely, of the KOs affecting maturation after 15 days, 30% (13/43) resulted in immature GPLCs and 70% (30/43) mature (Figure 2B; Table 1). Of note, 10% (17 KOs) of top targets altering GPLC maturation were members of a curated list of 581 "OMIM genes" known to cause monogenic disorders of skeletal growth (www.omim.org),[5] more than expected by chance (Fisher's exact test $p < 1.18 \times 10^{-6}$, Table 2).

Of the 140 genes most strongly affecting GPLC maturation, at least 13 are in pathways linked to skeletal growth, including two negative regulators of the Indian hedgehog (IHH) signaling pathway: suppressor of fused (*Sufu*) and the hedgehog receptor, patched-1 (*Ptch1*). Murine KO models of *Sufu* and *Ptch1* demonstrate disrupted growth-plate morphology.[17] In our assay, KO of *Sufu* or *Ptch1* led to premature chondrocyte maturation (Figures 2A and 2B), presumably due to increased hedgehog signaling. Several other genes most strongly implicated by our assay encode members of the H3K27 methyltransferase polycomb repressive complex (PRC2), Eed, Ezh2, and Suz12 (Figure 2; Table 1); these genes are mutated in human overgrowth syndromes[37–39] and have demonstrated disrupted growth-plate morphology in KO animal models.[40,41] We also observed enrichment in KEGG pathways for Wnt signaling, Hedgehog signaling, ubiquitin-mediated proteolysis, TGF-β/BMP signaling, and Hippo signaling pathways (false discovery rate [FDR] <0.015; Figure 2C). Taken together, these results demonstrate the ability of our assay to effectively highlight genes and pathways of clear relevance to growth-plate chondrocyte maturation and skeletal growth.

Genes significantly affecting chondrocyte maturation *in vitro* overlap with GWAS height-associated genes and independently predict height heritability

We next investigated whether genes significantly affecting chondrocyte maturation were orthogonally implicated by height GWASs and whether screening data could be used to prioritize genes likely mediating observed GWAS associations. We performed a meta-analysis of our primary screening (Figure 2D) and identified genes that both (1) significantly altered the maturation of GPLCs ($p < 0.01$) and (2) were highly prioritized by the benchmarker gene prioritization method[11] combined with three methods—PoPS,[10] MAGMA,[9] and DEPICT[8]—across two different height GWASs by Yengo et al.[3,4] (Figure 3A). We found a significant enrichment in KOs leading to early GPLC maturation and genes prioritized by both 2018 and 2022 height GWASs when intersecting our meta-analyzed screening data ($p < 0.01$) with GWAS-prioritized genes (binomial test $p < 5.24 \times 10^{-8}$ and $p < 8.06 \times 10^{-5}$, respectively; Figure 3B; Table S1). The overlapping set of 228 GWAS-prioritized genes is responsible for most of the enrichment (binomial test $p < 4.73 \times 10^{-6}$). We examined whether the association between KOs and GWAS-prioritized

Table 1. KOs affecting chondrocyte maturation on genome-wide screening

	Gene symbol	Official full name	Significance (neg. log p value)	Immature	Mature	Significant at D4	Significant at D15	Proliferation (D0 vs. D15)	Height GWAS gene	OMIM gene	Murine length (MGI)	Murine length (IMPC)	PubMed phenotype	Human height (HPO)	Rare-variant pLoF height burden (Genebass)
1	CD200	CD200 molecule	11.1	•	–	•	•	–	–	–	–	–	–	–	–
2	SUFU	SUFU negative regulator of hedgehog signaling	10.8	–	•	•	•	–	•	–	–	ns	–	▼/▲	–
3	EED	embryonic ectoderm development	9.3	–	•	•	•	–	–	–	–	–	–	▲	–
4	FKBP1A	FKBP prolyl isomerase 1A	8.9	–	•	–	•	–	–	–	–	–	–	–	–
5	PTCH1	patched 1	8.5	–	•	•	•	▲	•	•	–	–	length ▼; Hsu et al.; Mak et al.[17,18]	▼	▼
6	EZH2	histone-lysine N-methyltransferase EZH2	8.4	–	•	•	–	–	•	•	–	ns	–	▲	–
7	DOT1L	DOT1-like histone lysine methyltransferase	7.9	–	•	•	–	–	•	–	–	ns	–	–	–
8	STRAP	serine-threonine kinase receptor-associated protein	7.5	–	•	•	–	▼	–	–	–	ns	–	–	–
9	ARRB2	β-arrestin-2	7.1	–	•	•	•	–	–	–	–	–	–	–	–
10	FUZ	protein fuzzy homolog	6.5	–	•	–	•	–	–	–	–	ns	–	–	–
11	SUZ12	polycomb protein Suz12	6.4	–	•	•	–	–	–	–	–	–	–	–	–
12	PIAS1	protein inhibitor of activated Stat 1	6.4	–	•	•	–	–	–	–	–	–	–	▲	–
13	CSNK2B	casein kinase II subunit β	6.4	–	•	–	•	–	–	–	–	–	–	–	–
14	ALDH2	aldehyde dehydrogenase 2	6.3	–	•	•	–	–	–	–	–	ns	–	–	–
15	BRD2	bromodomain-containing protein 2	6.2	•	–	•	–	–	–	–	–	ns	–	–	–
16	UROD	uroporphyrinogen decarboxylase	5.8	–	•	•	–	–	–	–	–	–	–	–	–
17	ATP2B1	plasma membrane calcium-transporting ATPase 1	5.7	•	–	•	–	–	–	–	–	ns	–	–	–
18	PTBP1	polypyrimidine tract binding protein 1	5.7	–	•	•	–	–	–	–	–	–	–	–	–
19	CDYL	chromodomain Y-like protein	5.6	–	•	•	–	–	–	–	–	ns	–	–	–

(*Continued on next page*)

Table 1. ***Continued***

	Gene symbol	Official full name	Significance (neg. log p value)	Immature	Mature	Significant at D4	Significant at D15	Proliferation (D0 vs. D15)	Height GWAS gene	OMIM gene	Murine length (MGI)	Murine length (IMPC)	PubMed phenotype	Human height (HPO)	Rare-variant pLoF height burden (Genebass)
20	EDC4	enhancer of mRNA-decapping protein 4	5.3	–	•	–	•	–	–	–	–	ns	–	–	–
21	CCM2	cerebral cavernous malformations protein 2 homolog	5.3	•	–	•	–	–	–	–	–	–	–	–	–
22	GNAS	GNAS complex locus	5.2	–	•	•	–	–	–	•	▼	–	short limbs; Sakamoto et al.[19]	▼	–
23	WDPCP	WD repeat-containing and planar cell polarity effector protein fritz homolog	5.2	–	•	–	•	–	–	–	–	–	–	▼	–
24	MIB1	E3 ubiquitin-protein ligase mind-bomb	5.0	–	•	–	•	–	•	–	–	–	–	–	–
25	YWHAE	tyrosine 3-monooxygenase/ tryptophan 5-monooxygenase activation protein ε	5.0	•	–	•	–	–	–	–	–	–	–	▲	–
26	RPS28	small subunit ribosomal protein s28e	4.9	•	–	•	–	▼	–	•	–	–	–	▼	–
27	RUNX2	Runt-related transcription factor 2	4.9	•	–	•	–	–	•	•	–	ns	short limbs; Rashid et al.[20]	▼	–
28	SMAD6	mothers against decapentaplegic homolog 6	4.8	–	•	•	•	–	•	–	–	–	–	–	–
29	METTL14	N6-adenosine-methyltransferase non-catalytic subunit	4.8	•	–	•	•	–	–	–	–	ns	–	–	–
30	RAB7	RAB7, member RAS oncogene family	4.8	•	–	•	–	▼	–	–	–	–	–	–	–
31	CTDNEP1	CTD nuclear envelope phosphatase 1	4.8	–	•	–	•	–	–	–	–	–	–	–	–
32	VPS29	vacuolar protein sorting-associated protein 29	4.7	•	–	•	–	▼	–	–	–	–	–	–	–

(*Continued on next page*)

Table 1. *Continued*

	Gene symbol	Official full name	Significance (neg. log p value)	Immature	Mature	Significant at D4	Significant at D15	Proliferation (D0 vs. D15)	Height GWAS gene	OMIM gene	Murine length (MGI)	Murine length (IMPC)	PubMed phenotype	Human height (HPO)	Rare-variant pLoF height burden (Genebass)
33	PDCD10	programmed cell death protein 10	4.7	•	–	•	•	–	–	–	–	–	–	–	–
34	CHD8	chromodomain-helicase-DNA-binding protein 8	4.7	•	–	•	–	–	–	–	–	–	–	▲	–
35	PRKAR1A	protein kinase, cAMP-dependent regulatory, type I, α	4.6	•	–	•	•	▲	–	•	▼	–	short limbs; Le Stunff et al.[21]	▼	–
36	MED26	mediator of RNA polymerase II transcription subunit 26	4.5	•	–	•	•	–	–	–	–	–	–	–	–
37	KDM1A	lysine (K)-specific demethylase 1A	4.5	•	–	•	–	▲	–	–	–	ns	–	▼	–
38	COP1	E3 ubiquitin-protein ligase RFWD2	4.4	•	–	•	•	▲	–	–	–	–	–	–	–
39	FARSA	phenylalanyl-tRNA synthetase, α subunit	4.4	•	–	•	–	▼	–	–	–	ns	–	▼	–
40	FOXC1	forkhead box protein C1	4.3	•	–	•	–	–	•	–	–	–	–	–	–
41	PSMD14	proteasome 26S subunit, non-ATPase, 14	4.3	•	–	•	–	▼	–	–	–	ns	–	–	–
42	CTBP1	C-terminal-binding protein 1	4.3	–	•	•	–	–	–	–	–	–	–	▼/▲	–
43	MED12	mediator of RNA polymerase II transcription subunit 12	4.2	•	–	–	•	▲	–	–	–	–	–	▼/▲	–
44	CIC	protein capicua homolog	4.2	–	•	•	–	–	–	–	–	–	–	▲	–
45	EIF3H	eukaryotic translation initiation factor 3 subunit H	4.1	•	–	–	•	▲	–	–	–	ns	–	–	–
46	PIBF1	progesterone immunomodulatory binding factor 1	4.1	–	•	–	•	–	–	–	–	–	–	–	–

(*Continued on next page*)

Table 1. *Continued*

	Gene symbol	Official full name	Significance (neg. log p value)	Immature	Mature	Significant at D4	Significant at D15	Proliferation (D0 vs. D15)	Height GWAS gene	OMIM gene	Murine length (MGI)	Murine length (IMPC)	PubMed phenotype	Human height (HPO)	Rare-variant pLoF height burden (Genebass)
47	TRAF3IP1	TRAF3-interacting protein 1	4.1	–	•	–	•	–	–	–	–	–	–	▼	–
48	EIF4E2	eukaryotic translation initiation factor 4E type 2	4.0	•	–	•	–	–	–	–	–	–	–	–	–
49	PSMC4	proteasome (prosome, macropain) 26S subunit, ATPase, 4	4.0	•	–	•	–	▼	–	–	–	–	–	–	–
50	SOX6	transcription factor sox5/6/13	4.0	–	•	•	–	–	–	–	–	–	–	–	–
51	KPNB1	karyopherin (importin) β1	4.0	•	–	•	–	▼	–	–	–	–	–	–	–
52	RALGAPB	Ral GTPase-activating protein, β subunit (non-catalytic)	4.0	–	•	•	–	–	–	–	–	ns	–	–	–
53	CTCF	transcriptional repressor CTCF	4.0	•	–	•	–	▼	•	–	–	–	–	▼	–
54	IFT172	intraflagellar transport protein 172 homolog	3.9	–	•	–	•	–	–	•	–	ns	–	▼	–
55	DDX27	probable ATP-dependent RNA helicase DDX27	3.9	•	–	•	–	▼	–	–	–	–	–	–	–
56	EMSY	Emsy, Brca2-interacting transcriptional repressor	3.9	•	–	•	–	–	–	–	–	–	–	–	–
57	GCN1	eIF-2α kinase activator GCN1	3.8	•	–	•	–	–	–	–	–	–	–	–	–
58	HNRNPC	heterogeneous nuclear ribonucleoproteins C1/C2	3.8	–	•	•	–	▼	–	–	–	–	–	–	–
59	PPP2R5D	serine/threonine-protein phosphatase 2A 56 kDa regulatory subunit	3.8	–	•	•	–	–	–	–	–	ns	–	–	–

(*Continued on next page*)

Table 1. *Continued*

	Gene symbol	Official full name	Significance (neg. log p value)	Immature	Mature	Significant at D4	Significant at D15	Proliferation (D0 vs. D15)	Height GWAS gene	OMIM gene	Murine length (MGI)	Murine length (IMPC)	PubMed phenotype	Human height (HPO)	Rare-variant pLoF height burden (Genebass)
60	UTP4	U3 small nucleolar RNA-associated protein 4 homolog	3.8	•	–	•	–	▼	–	–	–	–	–	–	–
61	WDR70	WD repeat domain 70	3.7	•	–	•	–	▼	–	–	–	–	–	–	▼
62	CSDE1	cold shock domain-containing protein E1	3.7	–	•	•	–	–	–	–	–	–	–	–	–
63	PAK1IP1	P21-activated protein kinase-interacting protein 1	3.7	•	–	•	–	▼	–	–	–	ns	–	–	–
64	GEMIN5	Gem-associated protein 5	3.7	•	–	•	–	▼	–	–	–	–	–	–	–
65	PFDN5	prefoldin α subunit	3.7	•	–	•	–	▼	–	–	–	ns	–	–	–
66	DBR1	lariat debranching enzyme	3.7	•	–	•	–	▼	–	–	–	–	–	–	–
67	SEC61B	protein transport protein Sec61 subunit β	3.7	•	–	•	–	▼	–	–	–	ns	–	–	–
68	BYSL	essential nuclear protein 1	3.7	•	–	•	–	▼	–	–	–	–	–	–	–
69	BBC3	Bcl-2-binding component 3	3.7	–	•	–	•	–	–	–	–	ns	–	–	–
70	TRP53	transformation related protein 53	3.6	–	•	•	–	▲	–	–	–	–	–	–	–
71	SWI5	DNA repair protein SWI5 homolog	3.6	•	–	•	–	–	–	–	–	–	–	–	–
72	RBPJ	recombination signal binding protein for immunoglobulin κ J region	3.6	–	•	•	–	–	–	•	–	–	–	ns	–
73	GSK3B	glycogen synthase kinase-3β	3.6	–	•	–	•	–	•	–	–	–	–	–	–
74	RPL13	large subunit ribosomal protein l13e	3.6	•	–	•	–	▼	–	•	–	–	–	▼	–
75	ACLY	ATP-citrate synthase	3.6	•	–	•	–	▼	–	–	–	–	–	–	–

(*Continued on next page*)

Table 1. ***Continued***

	Gene symbol	Official full name	Significance (neg. log p value)	Immature	Mature	Significant at D4	Significant at D15	Proliferation (D0 vs. D15)	Height GWAS gene	OMIM gene	Murine length (MGI)	Murine length (IMPC)	PubMed phenotype	Human height (HPO)	Rare-variant pLoF height burden (Genebass)
76	SMC2	structural maintenance of chromosomes protein 2	3.6	•	–	•	–	▼	–	–	–	–	–	–	–
77	SUV39H1	suppressor of variegation 3-9 1	3.6	–	•	•	–	–	–	–	–	–	–	–	–
78	AFDN	afadin, adherens junction formation factor	3.5	–	•	•	–	–	–	–	–	ns	–	–	–
79	KRIT1	Krev interaction trapped protein 1	3.5	•	–	•	–	–	–	–	–	ns	–	–	–
80	TSC2	Tsc complex subunit 2	3.5	•	–	•	•	–	–	–	–	–	–	–	–
81	MTF2	metal-response element-binding transcription factor 2	3.5	–	•	•	–	–	–	–	–	–	–	–	–
82	KIF3B	kinesin-like protein KIF3B	3.5	–	•	•	•	–	–	–	–	ns	–	–	–
83	DCUN1D3	defective in cullin neddylation 1, domain-containing 3	3.5	–	•	–	•	–	–	–	–	ns	–	–	–
84	BMPR2	bone morphogenetic protein receptor type-2	3.4	–	•	•	–	–	–	–	–	–	–	–	▼
85	NAA30	N(α)-acetyltransferase 30, NATC catalytic subunit	3.4	–	•	–	•	–	–	–	–	–	–	–	–
86	BTBD7	BTB/POZ domain-containing protein 7	3.4	–	•	–	•	–	–	–	–	–	–	–	–
87	COMMD6	COMM domain-containing protein 6	3.4	•	–	•	–	–	–	–	–	–	–	–	–
88	PHF12	PHD-finger protein 12	3.4	•	–	•	–	–	•	–	–	–	–	–	–

(*Continued on next page*)

Table 1. ***Continued***

	Gene symbol	Official full name	Significance (neg. log p value)	Immature	Mature	Significant at D4	Significant at D15	Proliferation (D0 vs. D15)	Height GWAS gene	OMIM gene	Murine length (MGI)	Murine length (IMPC)	PubMed phenotype	Human height (HPO)	Rare-variant pLoF height burden (Genebass)
89	RIOK1	serine/threonine-protein kinase RIO1	3.4	•	–	•	–	▼	–	–	–	–	–	–	–
90	RPS3	40S ribosomal protein S3	3.4	•	–	•	–	▼	–	–	–	–	–	–	–
91	MTMR3	myotubularin-related protein 3	3.4	•	–	•	–	–	–	–	–	–	–	–	–
92	LGR4	leucine-rich repeat-containing G-protein-coupled receptor 4	3.4	–	•	•	–	–	–	–	–	–	–	–	–
93	NIP7	60S ribosome subunit biogenesis protein NIP7 homolog	3.3	•	–	•	–	▼	–	–	–	–	–	–	–
94	IRF2	interferon regulatory factor 2	3.3	•	–	•	–	–	•	–	–	–	–	–	–
95	EIF2B2	translation initiation factor eIF-2B subunit β	3.3	•	–	•	–	▼	–	–	–	ns	–	–	–
96	WASHC1	WASH complex subunit 1	3.3	•	–	•	–	–	–	–	–	–	–	–	–
97	NUDT21	Nudix (nucleoside diphosphate linked moiety x)-type motif 21	3.3	•	–	•	–	▼	–	–	–	–	–	–	–
98	VHL	von Hippel-Lindau disease tumor suppressor	3.3	•	–	•	–	▼	–	–	–	–	length ▼; Mangiavini et al.[22]	–	–
99	MYH9	myosin, heavy polypeptide 9, non-muscle	3.3	–	•	–	•	▲	–	–	–	ns	–	–	–
100	PRPF19	pre-mRNA-processing factor 19	3.3	•	–	•	–	▼	–	–	–	–	–	–	–
101	TRAF3	TNF receptor-associated factor 3	3.3	•	–	•	–	–	–	–	–	–	–	–	–

(*Continued on next page*)

Table 1. ***Continued***

	Gene symbol	Official full name	Significance (neg. log p value)	Immature	Mature	Significant at D4	Significant at D15	Proliferation (D0 vs. D15)	Height GWAS gene	OMIM gene	Murine length (MGI)	Murine length (IMPC)	PubMed phenotype	Human height (HPO)	Rare-variant pLoF height burden (Genebass)
102	DCP2	mRNA-decapping enzyme subunit 2	3.3	–	•	•	–	–	–	–	–	ns	–	–	–
103	PTPN11	tyrosine-protein phosphatase non-receptor type 11	3.3	•	–	•	–	▼	–	•	▼/▲	–	length ▼; Wang et al.; Lapinski et al.[23,24]	▼	–
104	RPL37	large subunit ribosomal protein l37e	3.3	•	–	•	–	▼	–	–	–	–	–	–	–
105	HCFC2	host cell factor C2	3.3	•	–	•	–	–	–	–	–	–	–	–	–
106	NEDD4	neural precursor cell expressed, developmentally down-regulated 4	3.3	•	–	•	–	–	–	–	–	–	–	–	–
107	ATP6V1E1	ATPase, H+ transporting, l ysosomal V1 subunit E1	3.3	•	–	•	–	▼	–	–	–	ns	–	▼/▲	–
108	ATP5A1	ATP synthase, H+ transporting, mitochondrial F1 complex, α subunit 1	3.2	•	–	•	–	▼	–	–	–	▼	–	–	–
109	GTF2H2	general transcription factor II H, polypeptide 2	3.2	•	–	•	–	▼	–	–	–	ns	–	–	–
110	RPS2	small subunit ribosomal protein S2E	3.2	•	–	•	–	▼	–	–	–	–	–	–	–
111	LOC100041806	–	3.2	•	–	•	–	▼	–	–	–	–	–	–	–
112	RUVBL2	RuvB-like 2	3.2	•	–	•	–	▼	–	–	–	–	–	–	–
113	APC	APC, WNT signaling pathway regulator	3.2	•	–	•	–	–	–	–	▼	–	–	–	–
114	WRB (GET1)	guided entry of tail-anchored proteins factor 1	3.2	•	–	•	–	▼	–	–	–	ns	–	–	–

(*Continued on next page*)

Table 1. ***Continued***

	Gene symbol	Official full name	Significance (neg. log p value)	Immature	Mature	Significant at D4	Significant at D15	Proliferation (D0 vs. D15)	Height GWAS gene	OMIM gene	Murine length (MGI)	Murine length (IMPC)	PubMed phenotype	Human height (HPO)	Rare-variant pLoF height burden (Genebass)
115	UBA52	ubiquitin-60S ribosomal protein L40	3.2	•	–	•	–	▼	–	–	–	–	–	–	–
116	MASTL	microtubule-associated serine/threonine kinase-like	3.2	•	–	•	–	–	–	–	–	–	–	–	–
117	SNRPE	small nuclear ribonucleoprotein E	3.2	•	–	•	–	▼	–	–	–	–	–	–	–
118	BAMBI	BMP and activin membrane-bound inhibitor homolog	3.2	–	•	•	•	–	–	–	–	ns	–	–	–
119	EPHA2	ephrin type-A receptor 2	3.1	•	–	–	•	–	–	–	–	ns	–	–	–
120	EIF2S1	eukaryotic translation initiation factor 2, subunit 1α	3.1	•	–	•	–	▼	–	–	–	ns	–	–	–
121	PSMA6	proteasome subunit α type-6	3.1	•	–	•	–	▼	–	–	–	–	–	–	–
122	NSF	N-ethylmaleimide-sensitive fusion protein	3.1	•	–	•	–	▼	–	–	–	–	–	–	–
123	ACVR1	activin receptor type-1	3.1	–	•	–	•	–	–	•	–	ns	ns length, distal limb malform; Hildebrand et al.[25]	ns; Pignolo et al.[26]	–
124	FOPNL (CEP20)	LisH domain-containing protein FOPNL	3.1	–	•	–	•	–	–	–	–	–	–	–	–
125	DYNC1I2	cytoplasmic dynein 1 intermediate chain 2	3.1	•	–	•	–	▼	–	•	ns	ns	–	▼	–

(*Continued on next page*)

Table 1. ***Continued***

	Gene symbol	Official full name	Significance (neg. log p value)	Immature	Mature	Significant at D4	Significant at D15	Proliferation (D0 vs. D15)	Height GWAS gene	OMIM gene	Murine length (MGI)	Murine length (IMPC)	PubMed phenotype	Human height (HPO)	Rare-variant pLoF height burden (Genebass)
126	ISCU	iron-sulfur cluster assembly enzyme ISCU, mitochondrial	3.1	•	–	•	–	▼	–	–	–	–	–	–	–
127	COMMD5	COMM domain-containing protein 5	3.1	•	–	•	–	–	–	–	–	–	–	–	–
128	ACTR2	actin-related protein 2	3.1	•	–	•	–	▼	–	–	–	–	–	–	–
129	PRMT1	protein arginine N-methyltransferase 1	3.1	•	–	•	–	▼	–	–	–	ns	–	–	–
130	NRP2	neuropilin-2	3.1	–	•	–	•	–	–	–	–	–	–	–	–
131	ARHGEF11	Rho guanine nucleotide exchange factor (GEF) 11	3.1	–	•	–	•	–	–	–	–	–	–	–	–
132	IFT57	intraflagellar transport protein 57 homolog	3.1	–	•	–	•	–	–	–	–	–	–	▼	–
133	ATP6V0E	ATPase, H+ transporting, lysosomal V0 subunit E	3.1	•	–	•	–	▼	–	–	–	–	–	–	–
134	DNAJC13	DNAJ heat shock protein family (hsp40) member c13	3.1	•	–	•	–	▼	–	–	–	–	–	–	–
135	RAB39B	RAB39B, member RAS oncogene family	3.0	•	–	–	•	–	–	–	–	ns	–	▼	–
136	KDM2A	F-box and leucine-rich repeat protein 10/11	3.0	•	–	•	–	–	•	–	–	–	–	–	–
137	CPLANE2	REM2- and Rab-like small GTPase 1	3.0	–	•	–	•	–	–	–	–	–	–	–	–

(*Continued on next page*)

Table 1. ***Continued***

	Gene symbol	Official full name	Significance (neg. log p value)	Immature	Mature	Significant at D4	Significant at D15	Proliferation (D0 vs. D15)	Height GWAS gene	OMIM gene	Murine length (MGI)	Murine length (IMPC)	PubMed phenotype	Human height (HPO)	Rare-variant pLoF height burden (Genebass)
138	LEMD3	inner nuclear membrane protein Man1	3.0	–	•	–	•	–	–	•	–	ns	–	▼	–
139	NFIC	nuclear factor 1 C-type	2.9	•	–	•	–	–	•	–	–	–	–	–	–
140	SMURF2	E3 ubiquitin-protein ligase SMURF2	2.9	–	•	•	–	–	•	–	–	–	–	–	▼
141	WDR34	WD repeat-containing protein 34	2.9	–	•	–	•	–	–	–	–	–	–	–	–
142	DET1	de-etiolated homolog 1 (Arabidopsis)	2.9	•	–	–	•	▲	–	–	–	–	–	–	–
143	IFT52	intraflagellar transport protein 52 homolog	2.9	–	•	–	•	–	–	•	–	ns	–	▼	–
144	SOX9	transcription factor Sox9	2.9	•	–	•	–	–	•	•	▼	–	length ▼; Yap et al.[27]	▼	–
145	BRD4	bromodomain-containing protein 4	2.8	•	–	•	–	–	•	–	–	–	–	▼	–
146	TRPS1	transcriptional repressor GATA binding 1	2.8	–	•	•	–	–	•	•	–	ns	short limbs; Wuelling et al.[28]	▼	–
147	CBFB	core-binding factor subunit β	2.7	•	–	•	–	–	•	–	–	–	–	–	–
148	TFAP4	transcription factor AP-4	2.7	•	–	•	–	–	•	–	▼	ns	–	–	–
149	UNC5B	netrin receptor UNC5B	2.7	–	•	•	–	–	•	–	–	–	–	–	–
150	ARNT	aryl hydrocarbon receptor nuclear translocator	2.5	–	•	•	–	–	•	–	–	–	–	–	–
151	HDAC5	histone deacetylase 4/5	2.4	–	•	•	–	–	•	–	–	–	–	–	–
152	BPTF	bromodomain PHD-finger transcription factor	2.4	•	–	•	•	–	•	–	▼	▼	–	▼	–

(*Continued on next page*)

Table 1. ***Continued***

	Gene symbol	Official full name	Significance (neg. log p value)	Immature	Mature	Significant at D4	Significant at D15	Proliferation (D0 vs. D15)	Height GWAS gene	OMIM gene	Murine length (MGI)	Murine length (IMPC)	PubMed phenotype	Human height (HPO)	Rare-variant pLoF height burden (Genebass)
153	LOXL1	lysyl oxidase-like protein 1	2.3	–	•	•	–	–	•	–	–	–	–	–	▲
154	PLAGL1	pleiomorphic adenoma gene-like 1	2.3	–	•	•	–	–	•	–	–	–	–	–	–
155	PAX9	paired-box protein Pax-9	2.3	–	•	•	–	–	•	–	–	–	–	–	–
156	SETD5	SET domain-containing protein 5	2.3	•	–	•	–	–	•	–	–	ns	–	–	–
157	YAP1	transcriptional coactivator YAP1	2.1	–	•	•	–	▼	•	–	–	–	–	–	–
158	HOXA11	homeobox protein Hox-A11	2.1	–	•	•	–	–	•	–	–	–	–	–	–
159	LPAR1	lysophosphatidic acid receptor 1	2.1	•	–	•	–	▼	•	–	–	–	–	–	–
160	BMPR1A	bone morphogenetic protein receptor type-1A	2.1	•	–	•	–	–	•	–	–	–	–	▼	–
161	LRP6	low-density lipoprotein receptor-related protein 6	2.0	–	•	•	–	–	•	–	–	–	–	–	–
162	ANKRD11	ankyrin repeat domain-containing protein 11	2.0	•	–	•	–	–	•	•	▼	▼	–	▼	▼

We identified 162 KOs that significantly affected maturation after 4 or 15 days of culture, with 132 genes affecting maturation at day 4 and 44 genes at day (D) 15. The average negative $\log_{10}$ p value across three replicate screens is shown, with • indicating KOs significant on either day. KOs perturbed maturation in the same direction at both screening time points. Barcode proliferation or depletion between D0 and D4 or D15 is noted with ▲ for >2-fold increase and ▼ for >2-fold decrease, while "ns" indicates less than 2-fold change. Targets implicated in human height GWASs or known to cause skeletal disease per the OMIM database are indicated, along with murine KOs with increased or decreased body length in the Mouse Genome Informatics Database (MGI)[29] or International Mouse Phenotyping Consortium (IMPC)[30] or association of targets with tall or short stature in humans in the Human Phenotype Ontology Database (HPO)[31] where available. Last, the estimated direction of effect on human height (increased [▲] or decreased [▼]) of predicted loss-of-function (pLoF) as estimated by the Sequence Kernel Association Test (SKAT)[32] from GeneBass[33] using data from the UK Biobank is indicated for pLoF gene burdens that surpass the Bonferroni significance threshold (SKAT-O,[34] $p < 0.05/159$).

Table 2. Intersect of OMIM genes with genome-wide screening data

Day 4

Gene	OMIM no.	Full gene name	OMIM human phenotype	Murine phenotype	Maturation at D4	Proliferation (D0 vs. D4)
ANKRD11	611192	ankyrin repeat domain-containing protein 11	skeletal dysplasia, short stature	bone: ossification ▼[35] length: ▼[30]	▼	ns
DYNC1I2	603331	cytoplasmic dynein 1 intermediate chain 2	short stature, microcephaly	bone: ns[30] length: ns[30]	▼	ns
EZH2	601573	histone-lysine N-methyltransferase EZH2	advanced osseous maturation, tall stature	bone: greater vertebral no.[30] length: ns[30]	▲	ns
GNAS	139320	GNAS complex locus	skeletal dysplasia, short stature	bone: shortened proliferative zone, accelerated hypertrophy length: ▼,[29] short limbs[19]	▲	ns
PRKAR1A	188830	cAMP-dependent protein kinase type I-α regulatory subunit	skeletal dysplasia, short stature, brachydactyly	bone: shortened GP hypertrophic zone, larger proliferative zone length: short limbs[21]	▼	ns
PTCH1	601309	patched 1	skeletal dysplasia, short stature, growth delay	bone: chondrocyte hypertrophy inhibited length: ▼[17,18]	▲	ns
PTPN11	176876	tyrosine-protein phosphatase non-receptor type 11	skeletal dysplasia, short stature	bone: limb deformity length: ▼[23,24]	▼	ns
RBPJ	147183	recombination signal binding protein for immunoglobulin κ J region	skeletal dysplasia, terminal limb defects, normal stature	bone: ns[30] length: ns[30]	▲	ns
RPL13	113703	large subunit ribosomal protein l13e	skeletal dysplasia, short stature, delayed growth	not available	▼	ns
RPS28	603685	small subunit ribosomal protein s28e	mandibulofacial dysostosis, short stature	bone: ns; Dickinson et al.[30] length: ns; Dickinson et al.[30]	▼	ns
RUNX2	600211	Runt-related transcription factor 2	skeletal dysplasia, short stature, vertebral malformation	bone: mineral ▼; Dickinson et al.[30] length: ns; Dickinson et al.[30]; shortened limbs; Rashid et al.[20]	▼	ns
SOX9	608160	transcription factor Sox9 (Sox group E)	skeletal dysplasia, short-limb short stature	bone: premature ossification length: ▼; Yap et al.[27]	▼	ns
TRPS1	604386	transcriptional repressor GATA binding 1	skeletal dysplasia, short-limb short stature	bone: delayed ossification; Malik et al.[36] length: ns; Dickinson et al.[30]; shortened limbs; Wuelling et al.[28]	▲	ns

Day 15

Gene	OMIM no.	Full gene name	OMIM human phenotype	Murine phenotype	Maturation at D15	Proliferation (D0 vs. D15)
ACVR1	102576	activin receptor type-1	fibrodysplasia ossificans progressive, normal stature	bone: ns; Dickinson et al.[30]; malformed limbs; Hildebrand et al.[25] length: ns; Dickinson et al.[30]; ns; Hildebrand et al.[25]	▲	ns
IFT172	607386	intraflagellar transport protein 172 homolog	skeletal dysplasia, short stature	bone: ns; Dickinson et al.[30] length: ns; Dickinson et al.[30]	▲	ns
IFT52	617094	intraflagellar transport protein 52 homolog	skeletal dysplasia, short stature	bone: ns; Dickinson et al.[30] length: ns; Dickinson et al.[30]	▲	ns
LEMD3	607844	inner nuclear membrane protein Man1	proportionate short stature, osteopoikilosis	bone: ns; Dickinson et al.[30] length: ns; Dickinson et al.[30]	▲	ns
PRKAR1A	188830	cAMP-dependent protein kinase type I-α regulatory subunit	skeletal dysplasia, short stature, brachydactyly	bone: shortened GP hypertrophic zone, larger proliferative zone length: short limbs; Le Stunff et al.[21]	▼	▲
PTCH1	601309	patched 1	skeletal dysplasia, short stature, growth delay	bone: chondrocyte hypertrophy inhibited length: ▼; Hsu et al.; Mak et al.[17,18]	▲	▲

The categorized genes are significant on genome-wide screening ($p < 0.01$) and belong to a curated list of OMIM genes known to cause human skeletal disease.[5] KO mouse phenotypes for bone and length are noted, where available. Maturation status on genome-wide screening is delineated (increased [▲], Z score >0; decreased [▼], Z score <0). Proliferation or depletion of barcodes between D0 and D4 or D15 is noted if >2-fold increased (▲) or >2-fold decreased (▼); "ns" indicates less than 2-fold change in barcode count.

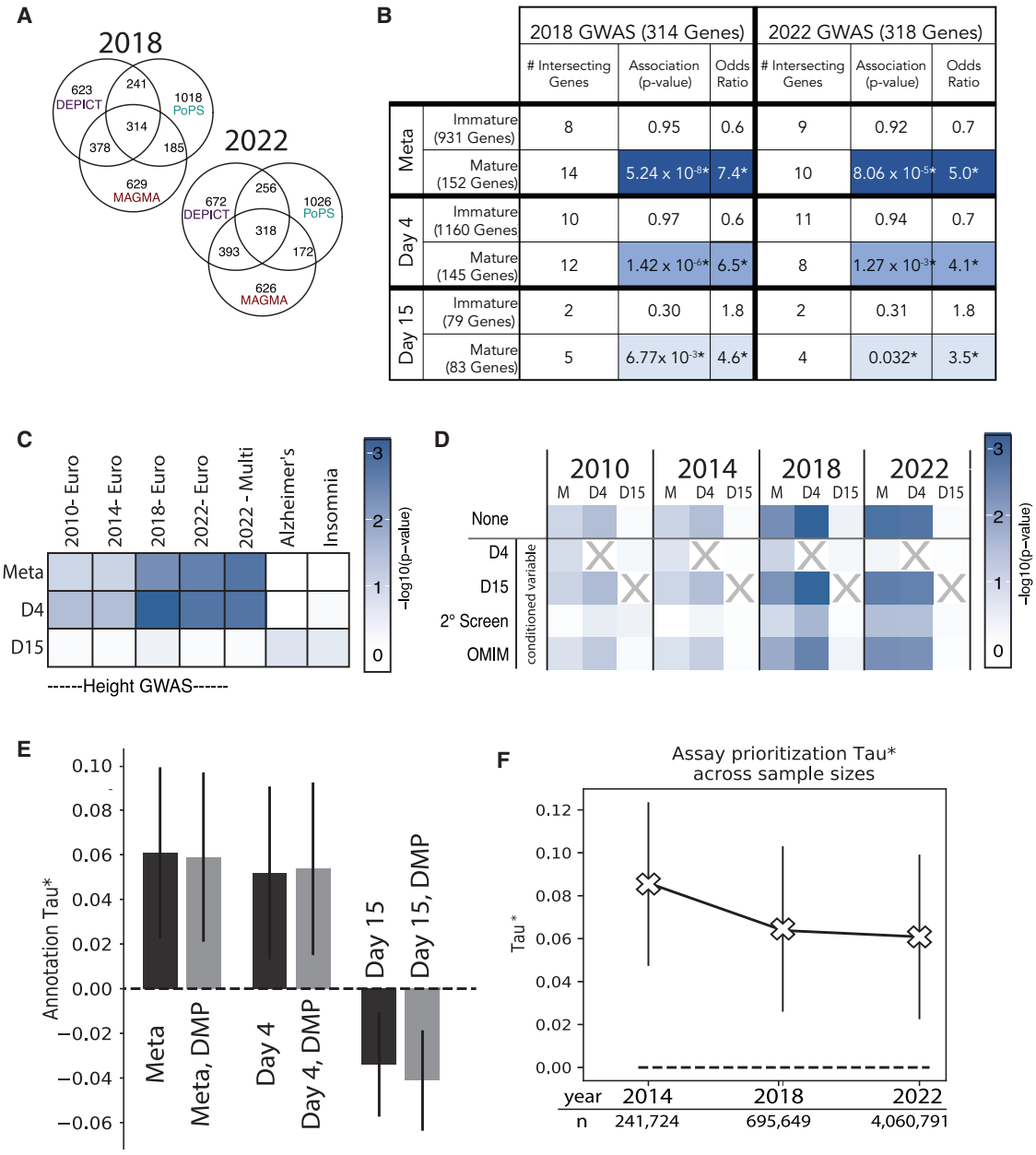

Figure 3. Genes significantly affecting chondrocyte maturation *in vitro* overlap with GWAS height genes and independently predict height heritability not captured by current GWAS gene assignment algorithms

(A) Comparison of gene counts highlighted by prioritization methods DEPICT (D), MAGMA (M), and PoPS (P) on height GWASs by Yengo et al.[3,4].

(B) Results of two-tailed binomial test evaluating the overlap (no. of intersecting genes) between significant GPLC KOs and 2018 or 2022 height GWAS DMP-prioritized genes. P values show significance of this association. Odds ratios are also shown.

(C) MAGMA gene set analysis comparing significance on GPLC KO screening with four successively published height GWASs (2010, 2014, 2018, 2022 European only; 2022 multi-ancestry), and GWASs hypothesized to have no association with our screening data (Alzheimer's disease, insomnia). MAGMA gene set association $-\log_{10}$ p values are shown in a color gradient, with darker blue indicating higher significance and white indicating no significance.

(D) MAGMA conditional gene set analysis, conditioning on D4 and D15 *Z* score absolute values, inclusion in the 162 genes selected for secondary screening, and inclusion in a list of OMIM genes.[5] MAGMA conditional gene set association $-\log_{10}$ p values are shown in a color gradient, with darker blue indicating higher significance and white indicating no significance.

(E) LD score regression comparing the partitioned heritability enrichment of genes prioritized by different time points (Tau*, standardized change of the per-SNP heritability per SD change in annotation, conditional on annotations in the model; lines note standard errors). LDSC run using baseline annotation; in addition, a binarized gene set enrichment analysis (GSEA) intersect was included with the baseline annotations for bars marked "DMP" (DEPICT/MAGMA/PoPS).

(F) sLDSC partitioned heritability enrichment among multiple height GWASs of genes prioritized by a meta-analysis of days 4 and 15 (Tau*, lines mark standard errors).[42]

genes was influenced by the day of screening. Enrichment was highest at day 4, where 12/145 KOs leading to early chondrocyte maturation were implicated by the 2018 GWAS (binomial test $p < 1.42 \times 10^{-6}$) and 8/145 were implicated by the 2022 GWAS (binomial test $p < 1.27 \times 10^{-3}$; Table S1). At day 15, 5/83 KOs leading to early chondrocyte maturation were 2018-GWAS implicated (binomial test $p < 6.77 \times 10^{-3}$) and 4/83 were 2022-GWAS implicated (binomial test $p < 0.032$; Figure 3B; Table S1). Enrichment at both time points appeared to be driven by the 228 genes prioritized from both GWASs, with significant enrichment observed at both time points (day 4 binomial test $p < 1.73 \times 10^{-3}$, day 15 binomial test $p < 0.0108$). Highly prioritized genes from height GWASs (2018 and 2022) were enriched among the genes that most strongly altered chondrocyte maturation in our screen (Kolmogorov-Smirnov $p \leq 0.05$, D statistic ≥ 0.069; Figures S3A and S3B).

We next tested for correlation between KO-screen performance and height GWAS gene-based p values across the entire genome using MAGMA.[9] The association increased with increasing GWAS sample size, with a stronger association observed in the most recent height GWAS[4] of 5.4 million individuals of diverse ancestries ($p = 0.0018$; Figure 3C). No associations were observed with comparably large GWASs of Alzheimer's disease (n = 455,258)[43] or insomnia (n = 1,331,010).[44] To test whether the observed correlation was driven by KOs resulting in immature or mature chondrocytes, or by day 4 or 15 of screening, we conditioned on individual datasets in MAGMA. Conditioning on data from day 4, but not 15, resulted in a loss of association between KO-screen performance and GWAS-gene significance (Figure 3D), suggesting that KOs altering chondrocyte maturation on day 4 drive the association with height GWAS. Conditioning on KOs driving immature or mature chondrocyte phenotypes did not alter the association (Figure S3C). This differs from the binomial analysis (Figure 3B), which used a prioritized set of GWAS genes and implicated KOs driving a mature chondrocyte phenotype. While both methods implicate day 4 as highly associated with height GWASs, the contrasting results may suggest that computational GWAS gene prioritization favors early-maturing gene KOs, while the full GWAS results do not (Figures 3B and 3D). Last, we found that the association between KO-screen performance and GWAS gene-based p values is not influenced by genes known to cause skeletal disease: conditioning on a curated set of 581 OMIM genes[5] did not reduce the significance of the association (Figure 3D).

We next investigated whether genes implicated by the screening data could capture additional heritability from height GWASs not already captured by genes implicated by current GWAS gene prediction algorithms. Using LD-score regression to partition heritability, we confirmed that our screen is able to highlight relevant height genes: variants near genes that alter maturation in our meta-analyzed screening data have significantly elevated per-SNP heritability in height GWAS data (Meta $p = 0.00282$, Meta DEPICT, MAGMA, PoPS [DMP] $p = 0.001467$, day 4 $p = 0.00501$, day4 DMP $p = 0.0031149$, day 15 $p = 0.8892$, day 15 DMP $p = 0.9063$; Figure 3E). Furthermore, this elevated per-SNP heritability is still present after accounting for the genes that emerge from existing gene prioritization algorithms (Figure 3E, DMP). Across multiple sample sizes of GWASs, this finding remains significant and indistinguishable with current power (Figure 3F). Thus, genome-wide functional assays from relevant tissues, in this case chondrocytes, are useful in refining or extending results from widely used gene prioritization algorithms, reiterating the utility of our assay in implicating novel genetic regulators of chondrocyte maturation within GWAS loci.

Secondary maturation screening confirms 145 top targets and demonstrates concordance between both screening time points

To validate genes from primary screening, 162 genes (Table 1) were selected based on significance alone ($p < 0.001$) or significance and GWAS association ($p < 0.01$ and implicated by Yengo et al.[3] via PoPS, DEPICT, and MAGMA). A secondary screen was conducted using 10 guides per gene and 10-fold more cells per guide (Figure 1B). Three replicate screens per time point were performed, with strong LFC correlation observed at both day 4 and day 15, enabling data combination for analysis (Figure S4). Forty-seven controls with expression in GPLCs by RNA sequencing[5] but no observed effect in primary screening were also included.

Figure 4 shows the results of our secondary screening at 4 days (Figure 4A) and 15 days (Figure 4B). We demonstrate concordance between the screens at day 4 (Pearson's $r = 0.937$, Figure 4C) and day 15 (Pearson's $r = 0.652$, Figure 4D) and validation of our top targets. Removing outlier sgRNAs targeting the same gene only marginally altered our final prioritized gene list was (Figure S5A). Interestingly, we observe that 87.7% of KOs have a greater effect in the primary screen at day 4 and 66% at day 15, likely due in part to the "winner's curse" effect, although LFC values are not directly comparable across libraries of different sizes.[45] KOs perturbing chondrocyte maturation more than control KO genes and in the same direction as in the primary screen were considered "validated." In our secondary analysis, we observed that 90% (145/162) of genes were validated for at least one time point, with 83% (134/162) of KOs validated at day 4 (Figure S5B) and 62% (101/162) validated at day 15 (Figure S5C).

Because we hypothesized that height GWASs could be used to direct our mechanistic studies of chondrocyte maturation toward genes of human relevance, we selected additional genes from height GWASs for secondary screening. While all KOs with $p < 0.001$ were included due to their performance on primary screening, an additional 22 genes with $p < 0.01$ were included due to their connection to human height GWASs. Of these "GWAS genes," 86% (19/22 genes targeted) rescreened above the 47 genes that had no effect in primary screening and were included as negative controls. This rescreening rate is nearly identical to that seen for KOs selected solely using more stringent thresholds from primary screen performance (87%, 122/140 genes targeted). This result suggests that, when used in conjunction with *in vitro* mechanistic studies, data from large-scale human genetic studies can be useful to direct meaningful refinement of genome-wide screens.

Comparing the directionality of perturbation (immature vs. mature) between KOs altering chondrocyte maturation on days 4 and 15 of secondary screening, we observed that 86% of

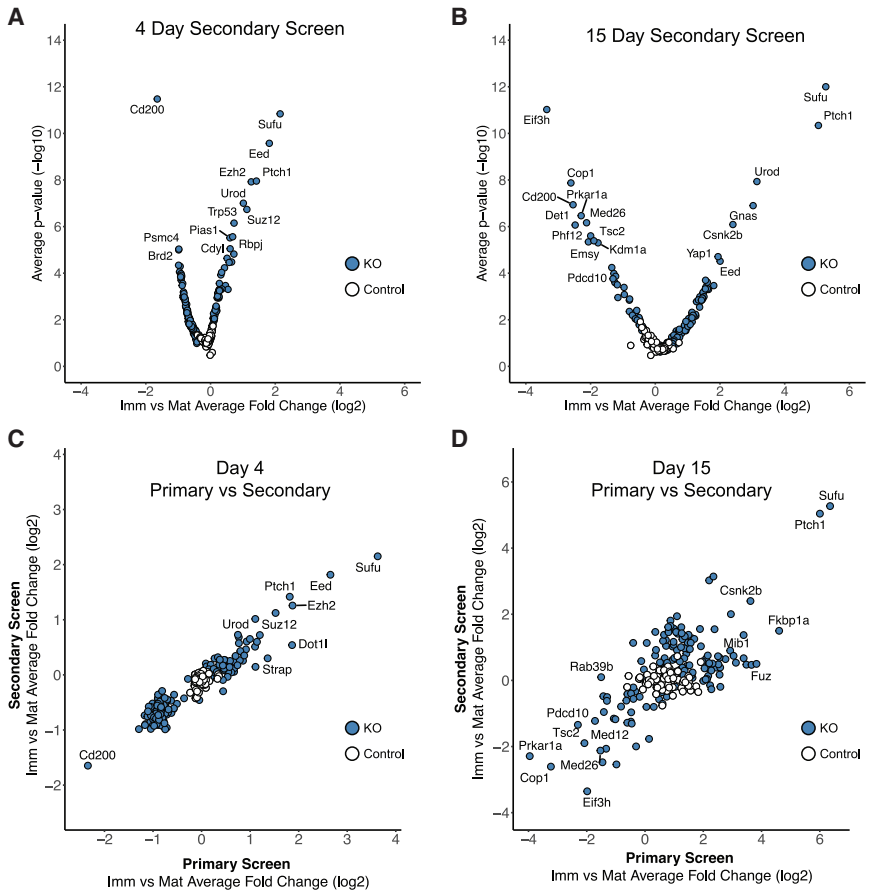

Figure 4. Secondary maturation screening confirms top targets from genome-wide screening and shows strong concordance between the screening time points

(A) KOs from 4-day secondary maturation screening. Volcano plot demonstrates average log2 fold change (LFC) between mature (top 10% CD-200-high cells) and immature (bottom 10% CD-200-low) KO populations across three replicate day 4 screens (Imm vs. Mat Average Fold Change [$\log_2$]), plotted against statistical significance (Average p value [$-\log_{10}$]). Gene KOs are shown in blue and non-targeting controls in white.

(B) KOs from 15-day secondary maturation screening.

(C) Direct comparison of 4-day primary and secondary screening.

(D) Direct comparison of 15-day primary and secondary screening.

KOs accelerating maturation at day 4 also accelerate maturation at day 15 (Figures 4A and 4B, positive LFC). Conversely, only 40% of KOs delaying maturation on day 4 also delay maturation by day 15, while 60% of KOs that were delayed at day 4 were accelerated by day 15 (Figures 4A and 4B). These results demonstrate robust concordance at both time points for KOs accelerating maturation, but only partial concordance for KOs delaying maturation. As might be expected, no KOs were found to result in a switch from advanced maturation at day 4 to delayed maturation at day 15. Globally, the most significant KOs perturbing chondrocyte maturation with the greatest effect size on secondary screening were those noted to be mature on both screening time points, including *Sufu* and *Ptch1*, members of the IHH signaling pathway, as well as *Eed*, *Ezh2*, and *Suz12*, which form polycomb repressive complexes with histone methyltransferase activity and have been shown to direct healthy endochondral ossification in animal models.[40,41]

Critical maturation targets are more clearly identified when accounting for cell proliferation over time

Our assay compares the top and bottom 10% of live CD-200-positive cells after 4 or 15 days in culture and thus can be considered a "competitive" screen, where KO perturbations alter the ability of cells to be included in the top or bottom 10%. Because chondrocytes are known to mature, hypertrophy, and undergo apoptosis, we hypothesized that some genes of relevance to chondrocyte maturation might be harder to detect in our assay due to depletion of maturing cells undergoing apoptosis after reaching the terminal hypertrophic stage of differentiation. Specifically, if KO of a particular gene causes immediate progression to the hypertrophic state, without multiple rounds of chondrocyte proliferation, such a KO might be difficult to detect as enriched among the top 10% most mature chondrocytes, due to the low number of CD-200-high cells collected for that KO. Conversely, KOs that increased proliferation during the assay might show greater statistical significance in our screen, due to the competitive advantage that proliferation provides. In addition, we also hypothesized that changes in proliferation might be accompanied by changes in maturation, since chondrocytes in the growth plate are known to first proliferate, then hypertrophy.

To begin to investigate this possibility, we sequenced unsorted secondary KO libraries at days 0, 4, and 15. No significant changes were observed in barcode prevalence corresponding to individual genes at day 4, with all counts within one LFC compared with day 0 (Figure 5A), such that KOs were not included or excluded in the top/bottom 10% due to cell depletion or proliferation. However, after 15 days, there was a significant shift in the unsorted cell distribution, with 9/162 (5.6%) KOs showing >2-fold expansion and 51/162 (31.4%) KOs showing >2-fold depletion (Figure 5A). We then assessed for a consistent relationship between proliferation and maturation in our assay, reflecting a biological link between the two processes in growth-plate chondrocytes. Using a positive or negative change in barcode count as a surrogate for KO cell proliferation or depletion, respectively, we asked whether groups of KOs in our secondary screen drove particular patterns of proliferation and maturation. Figure 5B reveals two primary patterns: most KOs (71.7%, 81/113) leading to chondrocyte maturation at day 15

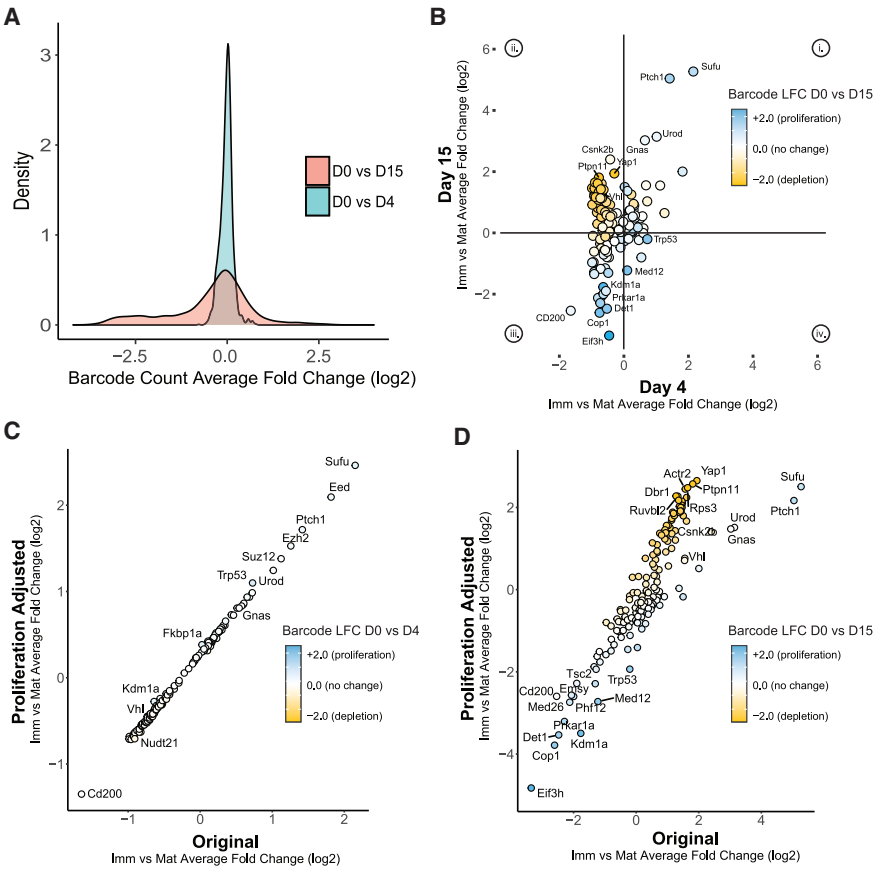

Figure 5. Critical maturation targets are prioritized when accounting for cell proliferation over time

(A) Density plot showing distribution of sgRNA barcode count average fold change (log_2), comparing representation between 0 and 4 or 15 days in culture.

(B) Secondary screening KOs, stratified by Imm vs. Mat average fold change (log_2) at day 4 vs. day 15, colored according to fold change in barcode count to illustrate whether KOs proliferated (blue), depleted (yellow), or did not change (white) between plating (day 0) and day 15.

(C) Proliferation-adjusted maturation LFC plotted against original maturation LFC at day 4 (Imm vs. Mat average fold change [log_2]). Adjusted maturation changes were calculated by principal component analysis (PCA) as described in the STAR Methods. KOs are colored by barcode proliferation (blue) or depletion (yellow) between day 0 and day 4.

(D) Proliferation-adjusted LFC for day 15 screening was plotted against original LFC (Imm vs. Mat average fold change [log_2] values). KOs are colored by barcode proliferation (blue) or depletion (yellow) between day 0 and day 15.

are also slightly immature at day 4 and are depleted between D0 and D15 (Figure 5B, quadrant ii contains mostly yellow circles indicating depletion over time). Conversely, most KOs that lead to immature chondrocytes at day 15 were also immature at day 4 and have increased proliferation over 15 days in culture (Figure 5B, quadrant iii has mostly blue circles indicating increased cell numbers). Thus, we observed that KO cells held in the immature state are more proliferative, while those leading to GPLC maturation are relatively depleted over 15 days in culture. An exception to this trend is two KOs, *Sufu* and *Ptch1*, which caused accelerated maturation at days 4 and 15, along with proliferation between days 0 and 15. These results are consistent with the action of these KOs to enhance IHH signaling, which has been shown to drive chondrocyte proliferation and, without the spatial regulation of PTHrP to delay hypertrophy seen *in vivo*, likely results in both enhanced proliferation and maturation in our assay.

To systematically account for the effect of proliferation in our maturation screen, we considered the impact of proliferation on the magnitude of change in maturation (LFC) driven by GPLC KOs. We performed principal component analysis (PCA) on data comparing change in KO cell counts over time with secondary maturation screening results at both day 4 (Figure S6A) and day 15 (Figure S6B). To adjust KOs for the effects of proliferation, principal component 1 (PC1) was calculated. As expected, on day 4 secondary screening, this adjustment did not change the rank order of our secondary screening targets, given the minimal effects on proliferation at this early time point (Figures 5C and S6C). Conversely, taking proliferation into account changed the LFC of KOs implicated in our day 15 screen (Figure 5D) and the rank order of our top maturation targets (Figure S6C); KOs depleted over time were adjusted to have a greater LFC, and KOs proliferating over time were adjusted to have a lower LFC. Here, we again observed that the majority of genes ranking higher after accounting for proliferation were those that result in maturation of chondrocytes. Thus, by accounting for proliferation, we were able to refine the ranking of genes whose KO altered maturation. This reranking of genes may better detect the effect of KOs on maturation despite their depletion in the population. For example, *Yap1* (encoding Yes-associated protein 1) and *Ptpn11* (encoding SH2 domain-containing protein tyrosine phosphatase 2) both become more strongly prioritized, with their adjusted ranks becoming first and second among the most significant KOs that accelerate maturation at day 15 (Figures 5D and S6C). Both *YAP1*[46] and *PTPN11*[23] are known to have important biological roles in the maturation of growth-plate chondrocytes, and mutations in *PTPN11* are the most common cause of short stature in the setting of Noonan syndrome (https://www.omim.org/entry/176876). These data indicate that considering both proliferation and maturation in the life cycle of the chondrocyte can improve estimates of maturation changes against a background of altered proliferation and also highlight genes with different biological impacts on chondrocyte proliferation and maturation.

To facilitate access to these data, we have built a searchable web resource for the research community at chondrocyte.shinyapps.io/Live.

DISCUSSION

Overview

This study couples human height GWASs with CRISPR-based functional genome-wide KO screening of chondrocytes to uncover genes and pathways related to human growth-plate maturation. Our comprehension of how height-associated GWAS variants affect height through the growth plate is restricted. Furthermore, progressing from associations in GWASs to the genes through which associated variants act remains a significant obstacle to fully harnessing the potential of GWAS, even for a phenotype such as height, where many relevant genes and pathways are known. Our study validated 145 genes as important for progression of chondrocyte maturation. In addition, we provide evidence that GWAS and mechanistic studies provide complementary information, pointing toward genes of importance to human health (Tables 2 and S1), and that the combination can prioritize genes more effectively than either approach in isolation.

Likewise, our data illustrate the value of functional studies in relevant tissues as orthogonal datasets to refine causal genes from GWASs. We found that genes prioritized by height GWASs from 2010 to 2022 were enriched among KOs most significantly affecting chondrocyte maturation, with increasing association seen with increasing GWAS sample size. Our functional screening independently predicted height heritability, even after accounting for genes assigned by existing algorithms (PoPS,[10] MAGMA,[9] DEPICT[8]). Therefore, our study suggests that genome-wide functional assays in chondrocytes could be a valuable tool for refining SNP-to-gene assignment in future height GWASs.

There is ongoing debate in the field of complex trait genetics about whether genetic effects predominantly act through many effector genes or on genes that in turn regulate a smaller set of direct effector genes. The "omnigenic" model[47] proposes that all genes in the genome that are expressed in a relevant cell type ("peripheral genes") contribute to the genetic basis of a trait, in this case height, through modulation of a set of direct effector "core" genes. We observed enrichment of genes with effects on maturation with gene-based association signals from GWAS, but the overlap between maturation genes and those implicated by computational algorithms (that use coexpression and other networks/pathways to prioritize genes from GWASs) is relatively small (<7% of prioritized genes) and represents a small fraction of all current height GWAS loci. Although our results do not speak directly to the omnigenic model, this could be seen as supporting the "polygenic" model of complex trait genetic architecture,[48] with substantial caveats about the likely difficulties in identifying the majority of relevant genes with either these computational models or our CRISPR screen. Regardless of the model, it is important to identify the effectors of skeletal growth that ultimately define human height and their mechanisms of action; our CRISPR screen and the cell-based assay that underlies it advance this goal by identifying genes involved in growth-plate maturation and providing a new way to explore mechanisms of action.

Interestingly, in our comparison with height GWASs, we observed that the highest enrichment of computationally prioritized GWAS genes was among KOs that led to early chondrocyte maturation. Many of the genes found to most robustly induce chondrocyte maturation when knocked out in our screen are also known to result in growth-plate chondrocyte phenotypes when mutated experimentally: *Sufu*,[17] *Eed*,[40] *Ptch1*,[17] *Runx2*,[49] *Yap1*,[46] and *Gnas*.[19] *Ptch1* and *Yap1* are also implicated by GWASs of height in 2018[3] and 2022.[4] Our observation of a stronger association between KOs leading to early chondrocyte maturation and genes prioritized from height GWASs suggests that genetic variants affecting the maturation of chondrocytes may have a greater influence on adult height, at least as assessed in height GWASs.

Patterns of maturation and proliferation emerge across early and late screening

To investigate genetic determinants of both chondrocyte immaturity and maturity, we paired early and late time points in our analysis. While we did not necessarily expect strong concordance between KO perturbations at both screening time points, aligning data from days 4 and 15 demonstrates a general concordance between the two time points (Figure 5B). Genes validated on both screening time points were more likely to be of known biological relevance. Specifically, KOs that matured early at day 4 and were still mature at day 15 (Figure 5B, quadrant ii) include *Sufu*, *Ptch1*, *Gnas*, *Eed*, *Ezh2*, and *Suz12*.

Murine KO models of *Sufu* and *Ptch1* demonstrate disrupted growth-plate morphology.[17] *Sufu*-deficient chondrocytes from Col2a1-Cre; Sufuf/f mice had increased hedgehog pathway activity, increased proliferation, and delayed differentiation. The phenotype of Col2a1-Cre; Ptch1f/f mice was similar to that of *Sufu*-deficient mice, with reduced hypertrophic zone length, increased proliferative zone size, abnormal chondrocyte proliferation and differentiation delay, and shortening of long bones.[17] By contrast, *Sufu*-deficient or *Ptch1*-deficient chondrocytes in our assay show both an increase in proliferation and enriched maturation. This difference between *in vitro* perturbation and *in vivo* observation is likely due to the lack of spatial architecture in cell culture that exists *in vivo*. *Sufu* and *Ptch1* are both negative regulators of the IHH signaling pathway. *Sufu* binds to and inhibits the activity of Gli proteins to regulate the level of IHH signaling in growth-plate chondrocytes, while *Ptch1* inhibits Smoothened (*Smo*), which transmits downstream signals. Loss of either *Sufu* or *Ptch1* leads to increased IHH signaling. In our screen, without the spatial, inhibitory regulation by *PTHrP* from the round cell layer,[50] cells with excessive IHH signaling may progress to hypertrophy.

Loss of *Gnas* is known to lead to premature hypertrophic differentiation of growth-plate chondrocytes.[19] Mice with chondrocyte-specific loss of Gsα manifest severe growth-plate defects, including a shortened proliferative zone and accelerated maturation of growth-plate chondrocytes. In our screening, we found that chondrocytes with loss of *Gnas* were abundant among mature populations at both day 4 and day 15. We did not observe a significant increase in proliferation with the loss of *Gnas*. The

correlation between *in vivo* and *in vitro* chondrocyte phenotype is more direct for *Gnas*-KO cells, indicating that the function of *Gnas* may be less dependent on spatial-temporal feedback loops between growth-plate layers *in situ*.

Other highly implicated genes in chondrocyte maturation at both day 4 and day 15 include members of the H3K27 methyltransferase polycomb repressive complex (PRC2), *Eed*, *Ezh2*, and *Suz12* (Figure 2; Table 1), which in humans are also mutated in overgrowth syndromes.[37–39] *Eed* deficiency in murine growth-plate chondrocytes results in growth defects with decreased chondrocyte proliferation and accelerated hypertrophic differentiation.[40] Combined loss of *Ezh1* and *Ezh2* in chondrocytes has been shown to severely impair skeletal growth in mice.[41] The study reported a significant reduction in chondrocyte proliferation and hypertrophy in Ezh1/2-KO mice and demonstrated that the reduced hypertrophy was mediated by increased insulin-like growth factor-1 (IGF-1) signaling. The findings suggest that the PRC2 complex plays a critical role in regulating both the proliferation and the hypertrophy of growth-plate chondrocytes. Our data show that loss of any member (*Eed*, *Ezh2*, and *Suz12*) resulted in increased chondrocyte maturation, and we observed no significant changes in proliferation over time (D0 vs. D15 Suz12 LFC −0.37; Eed LFC 0.39; Ezh2 LFC −0.74). In this case, discrepancies in chondrocyte behavior between our assay and mouse models may be attributed to the absence of essential hormonal signaling, such as IGF-1 in the case of PRC2 complex genes, that occurs *in vivo*.

Many KOs that were immature at day 4 also remained immature at day 15 (Figure 5B, quadrant iii). One such example is *Prkar1a*, which encodes the regulatory subunit of protein kinase A, a critical enzyme in the cAMP signaling pathway. Humans with loss-of-function mutations in Prkar1a exhibit Carney complex, a rare genetic disorder resulting from overactive adenylate cyclase and heightened proliferation of many cell types, including chondrocytes, resulting in osteochondromyxomas.[51,52] Studies have shown that loss of PRKAR1A results in chondrocyte proliferation and tumor formation in mice.[52] It is reasonable to predict that overdrive of PKA in *Prkar1a*-deficient chondrocytes will result increased proliferation (as seen in Carney complex) and decreased chondrocyte maturation, similar to the effects of PTHrP signaling via its receptor, a G-protein-coupled receptor (GPCR) that activates Gs, which in turn activates PKA.[53] This is congruent with the effect of *Prkar1a* KO to cause cell proliferation (barcodes increased 3.6-fold in culture by day 15) and to be immature in our chondrocyte screen (immature at D4 LFC −0.73, immature at D15 LFC −2.29).

A potential focus for future investigations is genes discovered in our screening that have limited or unknown connections to the growth plate in current literature. One such gene is *Det1*, an E3 ubiquitin ligase and member of the DET1-COP1 complex, required for ubiquitination and subsequent degradation of target proteins.[54] This complex is involved in the ubiquitination and degradation of several targets, including the proto-oncogene *Jun*, which has been shown separately to suppress the maturation of chondrocytes.[55] Thus, increased *Jun* from KO of *Det1* might plausibly result in immature chondrocytes (as observed on our screen). While, at the time of this study's publication, the search terms "Det1" and "chondrocyte" return 0 results, it is exciting to speculate that *Det1*, the KO of which drove an increase in immature chondrocytes on our screen, may be acting in the growth plate to suppress *Jun* and permit chondrocyte maturation.

KOs that led to enhanced chondrocyte maturation by day 15 can be further subdivided into those with and those without congruent maturation on day 4 screening. From these two groups, we observe that most of the KO GPLCs that showed maturation at both day 4 and day 15 did not have any advantage in proliferation (except for *Sufu* and *Ptch1*). However, KO GPLCs that matured only at day 15 were consistently reduced in culture over the 15-day period (Figure 5B, quadrant ii, yellow). Examples in this category include KO of von Hippel-Lindau (VHL) protein and protein tyrosine phosphatase non-receptor type 11 (Ptpn11). VHL is an E3 ubiquitin ligase that targets hypoxia-inducible factors. VHL loss during early limb development leads to shorter and delayed fetal bones due to impaired chondrocyte proliferation and differentiation.[22] The phenotype of decreased chondrocyte proliferation is congruent with the effect of VHL-KO in our assay (*Vhl*-KO barcodes were depleted over 2-fold by day 15). The phenotype of delayed chondrocyte maturation could be consistent with our observation that loss of VHL resulted in early chondrocyte immaturity and later increased maturation (immature at D4 LFC −0.73, mature at D15 LFC 1.13). Indeed, Mangiavini et al. observed early impairment of proliferation and profound delay of terminal differentiation in fetal KO mice, followed by early disappearance of the hypertrophic zone in post-natal animals, correlating with early cessation of long bone growth.[22]

Ptpn11 encodes the protein SH2-containing protein tyrosine phosphatase-2 (SHP2), which is recognized for its role in controlling the final development stage of growth-plate chondrocytes.[23,56] Loss of *Ptpn11* has been shown to expand the length of both the proliferative and the hypertrophic zones of mouse growth plates, in addition to disrupting the normally organized columnar structure of proliferating chondrocytes.[23,24] An increased proliferation of cells in the proliferative zone of KOs has also been described.[23] These results indicate the importance of the growth plate's spatial organization in the role of *Ptpn11* in chondrocytes, a factor that our assay does not take into account. Studies in chondrocyte pellet cultures have demonstrated that *Ptpn11*-KO cells exhibit elevated expression of genes associated with the proliferative and early hypertrophic zone, while the expression of late-hypertrophic genes is reduced.[56] The authors conclude that this shows a delay of terminal differentiation and prolonged proliferative/early hypertrophic phase. The complexities of pellet cell culture systems are also not replicated in our assay, although a plausible hypothesis consistent with both our results and previous work is that KO of *Ptpn11* could result in maintaining the early hypertrophic stage, preventing further proliferation, while delaying terminal differentiation (*Ptpn11*, immature at D4 LFC −0.77, mature at D15 LFC 1.81, and depleted nearly 6-fold in culture by day 15). These data illustrate that considering different patterns of maturation and proliferation at early and late time points can help elucidate different clusters of genes that affect chondrocyte maturation in the growth plate.

Limitations of the study

Although cell lines in culture cannot fully replicate the complex spatial, temporal landscape of the growth plate *in vivo*, our study used the GPLC cell line for genome-wide screening since obtaining primary cells from human growth plates is not currently feasible. While other chondrogenic cell lines, such as C28/I2, ATDC5, and C3H10T1/2, have been used for *in vitro* studies, they are not suitable for genome-wide growth-plate chondrocyte screening due to limitations of culture conditions and/or recapitulation of an articular cartilage phenotype.[57–65] Although use of the GPLC cell line enabled genome-wide screening, our chondrocyte maturation assay favors detection of KOs that have a proliferative advantage (most abundant KOs within the top/bottom 10% of mature/immature cells were selected). To account for this potential shortcoming, we considered background depletion of maturing cells. Furthermore, because our genome-wide screen applied stringent statistical thresholds for inclusion in secondary screening, we did not include all known genes affecting growth-plate chondrocyte maturation. Thus, relevant genes may have been missed using our approach of identifying KOs with a large perturbation effect. Last, our study assumes that gene-based p values, based on assignment of variants to the nearest gene, properly reflect the likelihood of being an effector gene from height GWASs. Although genes nearest to GWAS signals or with significant gene-based p values are enriched for effector genes, the relevant gene may be distant from GWAS signals, which may reduce our power to detect enrichment of effector genes among genes implicated by our assay.

Future directions

Our studies are the first to pair genome-wide functional maturation assays of chondrocytes with large-scale genetic studies of human height. Our studies illustrate how GWAS gene prioritization can be augmented by evaluating gene function within a tissue of biological relevance. The methodology established here provides an important technical resource for comparison of gene function in different stages of chondrocyte maturation and will aid in the ongoing translation of GWAS-associated SNPs to implicated causal genes regulating skeletal growth. Genes uncovered in our studies that are already known to mediate skeletal and growth disease validate the ability of our methods to uncover the biology underpinning growth-plate proliferation and maturation. Future mechanistic studies on each of the 145 validated screening targets may each contribute to a more complete understanding of the genetics of the growth plate. We hope that our current data will thus advance the field by providing a tool to advance future studies of individual genes and gene networks (available at chondrocyte.shinyapps.io/Live).

STAR★METHODS

Detailed methods are provided in the online version of this paper and include the following:

SUPPLEMENTAL INFORMATION

Supplemental information can be found online at https://doi.org/10.1016/j.xgen.2023.100299.

ACKNOWLEDGMENTS

We thank Dr. Vicki Rosen for the gift of the GPLC cell line. This work was supported by the Eunice Kennedy Shriver National Institute of Child Health and Human Development (NICHD K12HD052896), National Institute of Arthritis and Musculoskeletal and Skin Diseases (NIAMS K08AR078370), and National Institute of Diabetes and Digestive and Kidney Diseases (NIDDK R01DK075787) at the US National Institutes of Health (NIH) and by Boston Children's Hospital/Broad Institute Collaborative Project funding from the Boston Investment Conference.

AUTHOR CONTRIBUTIONS

Conceptualization, N.E.R., H.M.K., and J.N.H.; methodology, N.E.R., J.G.D., J.M.B., H.M.K., and J.N.H.; software, J.M.B.; validation, J.M.B. and N.E.R.; formal analysis, J.M.B., E.B., A.E., and N.E.R.; investigation, J.M.B. and N.E.R.; resources, J.G.D., E.B., A.E., L.Y., S.V., E.M., and the GIANT Consortium; writing – original draft, N.E.R., J.M.B., J.N.H., H.M.K., and E.B.; writing – review & editing, N.E.R., J.M.B., J.N.H., H.M.K., E.B., J.G.D., and L.Y.; visualization, J.M.B., E.B., and N.E.R.; supervision, N.E.R., H.M.K., and J.N.H.; project administration, N.E.R.; funding acquisition, N.E.R. and J.N.H..

DECLARATION OF INTERESTS

The authors declare no competing interests.

INCLUSION AND DIVERSITY

We support inclusive, diverse, and equitable conduct of research.

Received: October 26, 2022
Revised: December 14, 2022
Accepted: March 17, 2023
Published: April 14, 2023

REFERENCES

1. Lango Allen, H., Estrada, K., Lettre, G., Berndt, S.I., Weedon, M.N., Rivadeneira, F., Willer, C.J., Jackson, A.U., Vedantam, S., Raychaudhuri, S., et al. (2010). Hundreds of variants clustered in genomic loci and biological pathways affect human height. Nature *467*, 832–838. https://doi.org/10.1038/nature09410.

2. Wood, A.R., Esko, T., Yang, J., Vedantam, S., Pers, T.H., Gustafsson, S., Chu, A.Y., Estrada, K., Luan, J., Kutalik, Z., et al. (2014). Defining the role of common variation in the genomic and biological architecture of adult human height. Nat. Genet. *46*, 1173–1186. https://doi.org/10.1038/ng.3097.

3. Yengo, L., Sidorenko, J., Kemper, K.E., Zheng, Z., Wood, A.R., Weedon, M.N., Frayling, T.M., Hirschhorn, J., Yang, J., and Visscher, P.M.; GIANT Consortium (2018). Meta-analysis of genome-wide association studies for height and body mass index in approximately 700000 individuals of European ancestry. Hum. Mol. Genet. *27*, 3641–3649. https://doi.org/10.1093/hmg/ddy271.

4. Yengo, L., Vedantam, S., Marouli, E., Sidorenko, J., Bartell, E., Sakaue, S., Graff, M., Eliasen, A.U., Jiang, Y., Raghavan, S., et al. (2022). A saturated map of common genetic variants associated with human height from 5.4 million individuals of diverse ancestries. Preprint at bioRxiv. https://doi.org/10.1101/2022.01.07.475305.

5. Renthal, N.E., Nakka, P., Baronas, J.M., Kronenberg, H.M., and Hirschhorn, J.N. (2021). Genes with specificity for expression in the round cell layer of the growth plate are enriched in genomewide association study (GWAS) of human height. J. Bone Miner. Res. *36*, 2300–2308. https://doi.org/10.1002/jbmr.4408.

6. Lui, J.C., Nilsson, O., Chan, Y., Palmer, C.D., Andrade, A.C., Hirschhorn, J.N., and Baron, J. (2012). Synthesizing genome-wide association studies and expression microarray reveals novel genes that act in the human growth plate to modulate height. Hum. Mol. Genet. *21*, 5193–5201. https://doi.org/10.1093/hmg/dds347.

7. Gusev, A., Lee, S.H., Trynka, G., Finucane, H., Vilhjálmsson, B.J., Xu, H., Zang, C., Ripke, S., Bulik-Sullivan, B., Stahl, E., et al. (2014). Partitioning heritability of regulatory and cell-type-specific variants across 11 common diseases. Am. J. Hum. Genet. *95*, 535–552. https://doi.org/10.1016/j.ajhg.2014.10.004.

8. Pers, T.H., Karjalainen, J.M., Chan, Y., Westra, H.J., Wood, A.R., Yang, J., Lui, J.C., Vedantam, S., Gustafsson, S., Esko, T., et al. (2015). Biological interpretation of genome-wide association studies using predicted gene functions. Nat. Commun. *6*, 5890. https://doi.org/10.1038/ncomms6890.

9. de Leeuw, C.A., Mooij, J.M., Heskes, T., and Posthuma, D. (2015). MAGMA: generalized gene-set analysis of GWAS data. PLoS Comput. Biol. *11*, e1004219. https://doi.org/10.1371/journal.pcbi.1004219.

10. Weeks, E., Ulirsch, J., Cheng, N., Trippe, B., Fine, R., Miao, J., Patwardhan, T., Kanai, M., Nasser, J., Fulco, C., et al. (2020). Leveraging polygenic enrichments of gene features to predict genes underlying complex traits and diseases. Preprint at medRxiv. https://doi.org/10.1101/2020.09.08.20190561.

11. Fine, R.S., Pers, T.H., Amariuta, T., Raychaudhuri, S., and Hirschhorn, J.N. (2019). Benchmarker: an unbiased, association-data-driven strategy to evaluate gene prioritization algorithms. Am. J. Hum. Genet. *104*, 1025–1039. https://doi.org/10.1016/j.ajhg.2019.03.027.

12. Doench, J.G., Fusi, N., Sullender, M., Hegde, M., Vaimberg, E.W., Donovan, K.F., Smith, I., Tothova, Z., Wilen, C., Orchard, R., et al. (2016). Optimized sgRNA design to maximize activity and minimize off-target effects of CRISPR-Cas9. Nat. Biotechnol. *34*, 184–191. https://doi.org/10.1038/nbt.3437.

13. Jinek, M., Chylinski, K., Fonfara, I., Hauer, M., Doudna, J.A., and Charpentier, E. (2012). A programmable dual-RNA-guided DNA endonuclease in adaptive bacterial immunity. Science *337*, 816–821. https://doi.org/10.1126/science.1225829.

14. Rosen, V., Capparella, J., McQuaid, D., Cox, K., Thies, R.S., Song, J., and Wozney, J. (1993). Development of immortalized cells derived from 13DPC mouse limb buds as a system to study the effects of recombinant human bone morphogenetic protein-2 (rhBMP-2) on limb bud cell differentiation. Prog. Clin. Biol. Res. *383A*, 305–315.

15. Rosen, V., Nove, J., Song, J.J., Thies, R.S., Cox, K., and Wozney, J.M. (1994). Responsiveness of clonal limb bud cell lines to bone morphogenetic protein 2 reveals a sequential relationship between cartilage and bone cell phenotypes. J. Bone Miner. Res. *9*, 1759–1768. https://doi.org/10.1002/jbmr.5650091113.

16. Belluoccio, D., Etich, J., Rosenbaum, S., Frie, C., Grskovic, I., Stermann, J., Ehlen, H., Vogel, S., Zaucke, F., von der Mark, K., et al. (2010). Sorting of growth plate chondrocytes allows the isolation and characterization of cells of a defined differentiation status. J. Bone Miner. Res. *25*, 1267–1281. https://doi.org/10.1002/jbmr.30.

17. Hsu, S.H.C., Zhang, X., Yu, C., Li, Z.J., Wunder, J.S., Hui, C.C., and Alman, B.A. (2011). Kif7 promotes hedgehog signaling in growth plate chondrocytes by restricting the inhibitory function of Sufu. Development *138*, 3791–3801. https://doi.org/10.1242/dev.069492.

18. Mak, K.K., Chen, M.H., Day, T.F., Chuang, P.T., and Yang, Y. (2006). Wnt/beta-catenin signaling interacts differentially with Ihh signaling in controlling endochondral bone and synovial joint formation. Development *133*, 3695–3707. https://doi.org/10.1242/dev.02546.

19. Sakamoto, A., Chen, M., Kobayashi, T., Kronenberg, H.M., and Weinstein, L.S. (2005). Chondrocyte-specific knockout of the G protein G(s)alpha leads to epiphyseal and growth plate abnormalities and ectopic chondrocyte formation. J. Bone Miner. Res. *20*, 663–671. https://doi.org/10.1359/JBMR.041210.

20. Rashid, H., Chen, H., and Javed, A. (2021). Runx2 is required for hypertrophic chondrocyte mediated degradation of cartilage matrix during endochondral ossification. Matrix Biol. *12*, 100088. https://doi.org/10.1016/j.mbplus.2021.100088.

21. Le Stunff, C., Tilotta, F., Sadoine, J., Le Denmat, D., Briet, C., Motte, E., Clauser, E., Bougnères, P., Chaussain, C., and Silve, C. (2017). Knock-in of the recurrent R368X mutation of PRKAR1A that represses cAMP-dependent protein kinase A activation: a model of type 1 acrodysostosis. J. Bone Miner. Res. *32*, 333–346. https://doi.org/10.1002/jbmr.2987.

22. Mangiavini, L., Merceron, C., Araldi, E., Khatri, R., Gerard-O'Riley, R., Wilson, T.L., Rankin, E.B., Giaccia, A.J., and Schipani, E. (2014). Loss of VHL in mesenchymal progenitors of the limb bud alters multiple steps of endochondral bone development. Dev. Biol. *393*, 124–136. https://doi.org/10.1016/j.ydbio.2014.06.013.

23. Wang, L., Huang, J., Moore, D.C., Zuo, C., Wu, Q., Xie, L., von der Mark, K., Yuan, X., Chen, D., Warman, M.L., et al. (2017). SHP2 regulates the osteogenic fate of growth plate hypertrophic chondrocytes. Sci. Rep. *7*, 12699. https://doi.org/10.1038/s41598-017-12767-9.

24. Lapinski, P.E., Meyer, M.F., Feng, G.S., Kamiya, N., and King, P.D. (2013). Deletion of SHP-2 in mesenchymal stem cells causes growth retardation, limb and chest deformity, and calvarial defects in mice. Dis. Model. Mech. *6*, 1448–1458. https://doi.org/10.1242/dmm.012849.

25. Hildebrand, L., Schmidt-von Kegler, M., Walther, M., Seemann, P., and Stange, K. (2019). Limb specific Acvr1-knockout during embryogenesis in mice exhibits great toe malformation as seen in Fibrodysplasia Ossificans Progressiva (FOP). Dev. Dyn. *248*, 396–403. https://doi.org/10.1002/dvdy.24.

26. Pignolo, R.J., Baujat, G., Brown, M.A., De Cunto, C., Hsiao, E.C., Keen, R., Al Mukaddam, M., Le Quan Sang, K.H., Wilson, A., Marino, R., et al. (2022). The natural history of fibrodysplasia ossificans progressiva: a prospective, global 36-month study. Genet. Med. *24*, 2422–2433. https://doi.org/10.1016/j.gim.2022.08.013.

27. Yap, S.P., Xing, X., Kraus, P., Sivakamasundari, V., Chan, H.Y., and Lufkin, T. (2011). Generation of mice with a novel conditional null allele of the Sox9 gene. Biotechnol. Lett. *33*, 1551–1558. https://doi.org/10.1007/s10529-011-0608-6.

28. Wuelling, M., Kaiser, F.J., Buelens, L.A., Braunholz, D., Shivdasani, R.A., Depping, R., and Vortkamp, A. (2009). Trps1, a regulator of chondrocyte proliferation and differentiation, interacts with the activator form of Gli3. Dev. Biol. *328*, 40–53. https://doi.org/10.1016/j.ydbio.2009.01.012.

29. Smith, C.L., and Eppig, J.T. (2009). The mammalian phenotype ontology: enabling robust annotation and comparative analysis. Wiley Interdiscip. Rev. Syst. Biol. Med. *1*, 390–399. https://doi.org/10.1002/wsbm.44.

30. Dickinson, M.E., Flenniken, A.M., Ji, X., Teboul, L., Wong, M.D., White, J.K., Meehan, T.F., Weninger, W.J., Westerberg, H., Adissu, H., et al. (2016). High-throughput discovery of novel developmental phenotypes. Nature *537*, 508–514. https://doi.org/10.1038/nature19356.

31. Köhler, S., Gargano, M., Matentzoglu, N., Carmody, L.C., Lewis-Smith, D., Vasilevsky, N.A., Danis, D., Balagura, G., Baynam, G., Brower, A.M., et al. (2021). The human phenotype ontology in 2021. Nucleic Acids Res. *49*, D1207–D1217. https://doi.org/10.1093/nar/gkaa1043.

32. Wu, M.C., Lee, S., Cai, T., Li, Y., Boehnke, M., and Lin, X. (2011). Rare-variant association testing for sequencing data with the sequence kernel association test. Am. J. Hum. Genet. *89*, 82–93. https://doi.org/10.1016/j.ajhg.2011.05.029.

33. Karczewski, K.J., Solomonson, M., Chao, K.R., Goodrich, J.K., Tiao, G., Lu, W., Riley-Gillis, B.M., Tsai, E.A., Kim, H.I., Zheng, X., et al. (2022). Systematic single-variant and gene-based association testing of thousands of phenotypes in 394,841 UK Biobank exomes. Cell Genom. *2*, 100168.

34. Lee, S., Emond, M.J., Bamshad, M.J., Barnes, K.C., Rieder, M.J., Nickerson, D.A., NHLBI GO Exome Sequencing Project—ESP Lung Project Team; Christiani, D.C., Wurfel, M.M., and Lin, X. (2012). Optimal unified approach for rare-variant association testing with application to small-sample case-control whole-exome sequencing studies. Am. J. Hum. Genet. *91*, 224–237. https://doi.org/10.1016/j.ajhg.2012.06.007.

35. Roth, D.M., Baddam, P., Lin, H., Vidal-García, M., Aponte, J.D., De Souza, S.T., Godziuk, D., Watson, A.E.S., Footz, T., Schachter, N.F., et al. (2021). The chromatin regulator Ankrd11 controls palate and cranial bone development. Front. Cell Dev. Biol. *9*, 645386. https://doi.org/10.3389/fcell.2021.645386.

36. Malik, T.H., Von Stechow, D., Bronson, R.T., and Shivdasani, R.A. (2002). Deletion of the GATA domain of TRPS1 causes an absence of facial hair and provides new insights into the bone disorder in inherited trichorhino-phalangeal syndromes. Mol. Cell Biol. *22*, 8592–8600. https://doi.org/10.1128/MCB.22.24.8592-8600.2002.

37. Cohen, A.S.A., Tuysuz, B., Shen, Y., Bhalla, S.K., Jones, S.J.M., and Gibson, W.T. (2015). A novel mutation in EED associated with overgrowth. J. Hum. Genet. *60*, 339–342. https://doi.org/10.1038/jhg.2015.26.

38. Imagawa, E., Albuquerque, E.V.A., Isidor, B., Mitsuhashi, S., Mizuguchi, T., Miyatake, S., Takata, A., Miyake, N., Boguszewski, M.C.S., Boguszewski, C.L., et al. (2018). Novel SUZ12 mutations in Weaver-like syndrome. Clin. Genet. *94*, 461–466. https://doi.org/10.1111/cge.13415.

39. Griffiths, S., Loveday, C., Zachariou, A., Behan, L.A., Chandler, K., Cole, T., D'Arrigo, S., Dieckmann, A., Foster, A., Gibney, J., et al. (2019). EED and EZH2 constitutive variants: a study to expand the Cohen-Gibson syndrome phenotype and contrast it with Weaver syndrome. Am. J. Med. Genet. *179*, 588–594. https://doi.org/10.1002/ajmg.a.61066.

40. Mirzamohammadi, F., Papaioannou, G., Inloes, J.B., Rankin, E.B., Xie, H., Schipani, E., Orkin, S.H., and Kobayashi, T. (2016). Polycomb repressive complex 2 regulates skeletal growth by suppressing Wnt and TGF-beta signalling. Nat. Commun. *7*, 12047. https://doi.org/10.1038/ncomms12047.

41. Lui, J.C., Garrison, P., Nguyen, Q., Ad, M., Keembiyehetty, C., Chen, W., Jee, Y.H., Landman, E., Nilsson, O., Barnes, K.M., and Baron, J. (2016). EZH1 and EZH2 promote skeletal growth by repressing inhibitors of chondrocyte proliferation and hypertrophy. Nat. Commun. *7*, 13685. https://doi.org/10.1038/ncomms13685.

42. Gazal, S., Finucane, H.K., Furlotte, N.A., Loh, P.R., Palamara, P.F., Liu, X., Schoech, A., Bulik-Sullivan, B., Neale, B.M., Gusev, A., and Price, A.L. (2017). Linkage disequilibrium-dependent architecture of human complex traits shows action of negative selection. Nat. Genet. *49*, 1421–1427. https://doi.org/10.1038/ng.3954.

43. Jansen, I.E., Savage, J.E., Watanabe, K., Bryois, J., Williams, D.M., Steinberg, S., Sealock, J., Karlsson, I.K., Hägg, S., Athanasiu, L., et al. (2019). Genome-wide meta-analysis identifies new loci and functional pathways influencing Alzheimer's disease risk. Nat. Genet. *51*, 404–413. https://doi.org/10.1038/s41588-018-0311-9.

44. Jansen, P.R., Watanabe, K., Stringer, S., Skene, N., Bryois, J., Hammerschlag, A.R., de Leeuw, C.A., Benjamins, J.S., Muñoz-Manchado, A.B., Nagel, M., et al. (2019). Genome-wide analysis of insomnia in 1,331,010 individuals identifies new risk loci and functional pathways. Nat. Genet. *51*, 394–403. https://doi.org/10.1038/s41588-018-0333-3.

45. Xiao, R., and Boehnke, M. (2009). Quantifying and correcting for the winner's curse in genetic association studies. Genet. Epidemiol. *33*, 453–462. https://doi.org/10.1002/gepi.20398.

46. Deng, Y., Wu, A., Li, P., Li, G., Qin, L., Song, H., and Mak, K.K. (2016). Yap1 regulates multiple steps of chondrocyte differentiation during skeletal development and bone repair. Cell Rep. *14*, 2224–2237. https://doi.org/10.1016/j.celrep.2016.02.021.

47. Boyle, E.A., Li, Y.I., and Pritchard, J.K. (2017). An expanded view of complex traits: from polygenic to omnigenic. Cell *169*, 1177–1186. https://doi.org/10.1016/j.cell.2017.05.038.

48. Wray, N.R., Wijmenga, C., Sullivan, P.F., Yang, J., and Visscher, P.M. (2018). Common disease is more complex than implied by the core gene omnigenic model. Cell *173*, 1573–1580. https://doi.org/10.1016/j.cell.2018.05.051.

49. Takeda, S., Bonnamy, J.P., Owen, M.J., Ducy, P., and Karsenty, G. (2001). Continuous expression of Cbfa1 in nonhypertrophic chondrocytes uncovers its ability to induce hypertrophic chondrocyte differentiation and partially rescues Cbfa1-deficient mice. Genes Dev. *15*, 467–481. https://doi.org/10.1101/gad.845101.

50. Guo, J., Chung, U.I., Kondo, H., Bringhurst, F.R., and Kronenberg, H.M. (2002). The PTH/PTHrP receptor can delay chondrocyte hypertrophy in vivo without activating phospholipase C. Dev. Cell *3*, 183–194. https://doi.org/10.1016/s1534-5807(02)00218-6.

51. Carney, J.A., Gordon, H., Carpenter, P.C., Shenoy, B.V., and Go, V.L. (1985). The complex of myxomas, spotty pigmentation, and endocrine overactivity. Medicine *64*, 270–283. https://doi.org/10.1097/00005792-198507000-00007.

52. Kirschner, L.S., Kusewitt, D.F., Matyakhina, L., Towns, W.H., 2nd, Carney, J.A., Westphal, H., and Stratakis, C.A. (2005). A mouse model for the Carney complex tumor syndrome develops neoplasia in cyclic AMP-responsive tissues. Cancer Res. *65*, 4506–4514. https://doi.org/10.1158/0008-5472.CAN-05-0580.

53. Kobayashi, T., Chung, U.I., Schipani, E., Starbuck, M., Karsenty, G., Katagiri, T., Goad, D.L., Lanske, B., and Kronenberg, H.M. (2002). PTHrP and Indian hedgehog control differentiation of growth plate chondrocytes at multiple steps. Development *129*, 2977–2986. https://doi.org/10.1242/dev.129.12.2977.

54. Wertz, I.E., O'Rourke, K.M., Zhang, Z., Dornan, D., Arnott, D., Deshaies, R.J., and Dixit, V.M. (2004). Human De-etiolated-1 regulates c-Jun by assembling a CUL4A ubiquitin ligase. Science *303*, 1371–1374. https://doi.org/10.1126/science.1093549.

55. Kameda, T., Watanabe, H., and Iba, H. (1997). C-Jun and JunD suppress maturation of chondrocytes. Cell Growth Differ. *8*, 495–503.

56. Bowen, M.E., Ayturk, U.M., Kurek, K.C., Yang, W., and Warman, M.L. (2014). SHP2 regulates chondrocyte terminal differentiation, growth plate architecture and skeletal cell fates. PLoS Genet. *10*, e1004364. https://doi.org/10.1371/journal.pgen.1004364.

57. Goldring, M.B., Birkhead, J.R., Suen, L.F., Yamin, R., Mizuno, S., Glowacki, J., Arbiser, J.L., and Apperley, J.F. (1994). Interleukin-1 beta-modulated gene expression in immortalized human chondrocytes. J. Clin. Invest. *94*, 2307–2316. https://doi.org/10.1172/JCI117595.

58. Atsumi, T., Miwa, Y., Kimata, K., and Ikawa, Y. (1990). A chondrogenic cell line derived from a differentiating culture of AT805 teratocarcinoma cells. Cell Differ. Dev. *30*, 109–116. https://doi.org/10.1016/0922-3371(90)90079-c.

59. Reznikoff, C.A., Brankow, D.W., and Heidelberger, C. (1973). Establishment and characterization of a cloned line of C3H mouse embryo cells

sensitive to postconfluence inhibition of division. Cancer Res. *33*, 3231–3238.

60. Claassen, H., Schicht, M., Brandt, J., Reuse, K., Schädlich, R., Goldring, M.B., Guddat, S.S., Thate, A., and Paulsen, F. (2011). C-28/I2 and T/C-28a2 chondrocytes as well as human primary articular chondrocytes express sex hormone and insulin receptors–Useful cells in study of cartilage metabolism. Ann. Anat. *193*, 23–29. https://doi.org/10.1016/j.aanat.2010.09.005.

61. Quintiens, J., De Roover, A., Cornelis, F.M.F., Escribano-Núñez, A., Sermon, A., Pazmino, S., Monteagudo, S., and Lories, R.J. (2023). Hypoxia and Wnt signaling inversely regulate expression of chondroprotective molecule ANP32A in articular cartilage. Osteoarthritis Cartilage *31*, 507–518. https://doi.org/10.1016/j.joca.2022.10.019.

62. Kittl, M., Winklmayr, M., Preishuber-Pflügl, J., Strobl, V., Gaisberger, M., Ritter, M., and Jakab, M. (2021). Low pH attenuates apoptosis by suppressing the volume-sensitive outwardly rectifying (VSOR) chloride current in chondrocytes. Front. Cell Dev. Biol. *9*, 804105. https://doi.org/10.3389/fcell.2021.804105.

63. Li, G., Liu, S., Chen, Y., Xu, H., Qi, T., Xiong, A., Wang, D., Yu, F., Weng, J., and Zeng, H. (2023). Teriparatide ameliorates articular cartilage degradation and aberrant subchondral bone remodeling in DMM mice. J. Orthop. Translat. *38*, 241–255. https://doi.org/10.1016/j.jot.2022.10.015.

64. Roy, R., Kudryashov, V., Doty, S.B., Binderman, I., and Boskey, A.L. (2010). Differentiation and mineralization of murine mesenchymal C3H10T1/2 cells in micromass culture. Differentiation. *79*, 211–217. https://doi.org/10.1016/j.diff.2010.03.003.

65. Le, B.Q., Fernandes, H., Bouten, C.V.C., Karperien, M., van Blitterswijk, C., and de Boer, J. (2015). High-throughput screening assay for the identification of compounds enhancing collagenous extracellular matrix production by ATDC5 cells. Tissue Eng. Part C Methods *21*, 726–736. https://doi.org/10.1089/ten.TEC.2014.0088.

66. Joung, J., Konermann, S., Gootenberg, J.S., Abudayyeh, O.O., Platt, R.J., Brigham, M.D., Sanjana, N.E., and Zhang, F. (2017). Genome-scale CRISPR-Cas9 knockout and transcriptional activation screening. Nat. Protoc. *12*, 828–863. https://doi.org/10.1038/nprot.2017.016.

67. Dobin, A., Davis, C.A., Schlesinger, F., Drenkow, J., Zaleski, C., Jha, S., Batut, P., Chaisson, M., and Gingeras, T.R. (2013). STAR: ultrafast universal RNA-seq aligner. Bioinformatics *29*, 15–21. https://doi.org/10.1093/bioinformatics/bts635.

68. Putri, G.H., Anders, S., Pyl, P.T., Pimanda, J.E., and Zanini, F. (2022). Analysing high-throughput sequencing data in Python with HTSeq 2.0. Bioinformatics *38*, 2943–2945. https://doi.org/10.1093/bioinformatics/btac166.

69. Robinson, M.D., McCarthy, D.J., and Smyth, G.K. (2010). edgeR: a Bioconductor package for differential expression analysis of digital gene expression data. Bioinformatics *26*, 139–140. https://doi.org/10.1093/bioinformatics/btp616.

70. Pooled screen analysis tool - hypergeometric analysis. (2023). Broad Institute Genetic Perturbation Platform. https://portals.broadinstitute.org/gpp/public/.

71. Kanehisa, M., Furumichi, M., Sato, Y., Kawashima, M., and Ishiguro-Watanabe, M. (2023). KEGG for taxonomy-based analysis of pathways and genomes. Nucleic Acids Res. *51*, D587–D592. https://doi.org/10.1093/nar/gkac963.

72. Cunningham, F., Allen, J.E., Allen, J., Alvarez-Jarreta, J., Amode, M.R., Armean, I.M., Austine-Orimoloye, O., Azov, A.G., Barnes, I., Bennett, R., et al. (2022). Ensembl 2022. Nucleic Acids Res. *50*, D988–D995. https://doi.org/10.1093/nar/gkab1049.

73. Bulik-Sullivan, B., Finucane, H.K., Anttila, V., Gusev, A., Day, F.R., Loh, P.R., ReproGen Consortium; Psychiatric Genomics, C.; Genetic Consortium for Anorexia Nervosa of the Wellcome Trust Case Control; and Duncan, L., et al. (2015). An atlas of genetic correlations across human diseases and traits. Nat. Genet. *47*, 1236–1241. https://doi.org/10.1038/ng.3406.

STAR★METHODS

KEY RESOURCES TABLE

REAGENT or RESOURCE	SOURCE	IDENTIFIER
Antibodies/stains		
APC anti-mouse CD200 (OX2) Antibody	BioLegend	Catalog #: 123809, RRID:AB_10900996
Mouse Seroblock FcR	BioRad	Clone FCR4G8, RRID:AB_605398
DAPI (4',6-Diamidino-2-Phenylindole, Dihydrochloride)	Invitrogen	Catalog #: D1306
Bacterial and virus strains		
Lentivirus human immunodeficiency virus 1 (HIV 1)	Broad Institute	N/A
Cell culture reagents		
DMEM, high glucose	Gibco	Catalog #: 11965092
Fetal Bovine Serum, qualified, United States	Gibco	Catalog #: 26140087
Penicillin-Streptomycin (10,000 U/mL)	Gibco	Catalog #: 15140122
L-Ascorbic acid	Sigma-Aldrich	Catalog #: A5960
Insulin-Transferrin-Selenium (ITS -G) (100X)	Gibco	Catalog #: 41400045
Blasticidin S HCl (10 mg/mL)	Gibco	Catalog #: A1113903
Puromycin dihydrochloride	Sigma-Aldrich	Catalog #: P9620
Deposited data		
Mouse RNA sequencing data	This paper	GEO: GSE225796
CRISPR screen sequencing data	This paper	GEO: GSE225878
GPLC CD200 Sorted RNA sequencing data	This paper	GEO: GSE225879
Experimental models: Cell lines		
Growth Plate-Like Chondrocyte Cell Line (GPLC)	Vicki Rosen	PMID: 8302904, 7532346
Recombinant DNA		
Mouse CRISPR Knockout Pooled Library (Brie)	Broad Institute	Addgene Catalog #: 73633
pLX_311Cas9v2 (pXPR_111)	Broad Institute	N/A
Software and algorithms		
GPP Hypergeometric Distribution Tool	Broad Institute	https://portals.broadinstitute.org/gpp/public/
KEGG: Kyoto Encyclopedia of Genes and Genomes	Kanehisa Laboratories	https://www.genome.jp/kegg/
Benchmarker	Rebecca Fine	https://github.com/RebeccaFine/benchmarker
DEPICT	Pers Lab	https://github.com/perslab/depict
MAGMA (v1.07)	CNCR CTG Lab	https://ctg.cncr.nl/software/magma
PoPS	Finucane Lab	https://github.com/FinucaneLab/pops
LDSC (LD SCore) v1.0.1	Brendan Bulik-Sullivan	https://github.com/bulik/ldsc
R Statistical Software v4.1.0	R Core Team	https://cran.r-project.org/bin/windows/base/
Rstudio v2022.7.1.554	Rstudio Team	https://posit.co/
ggplot2 v3.3.5	tidyverse	https://ggplot2.tidyverse.org/
ggrepel v0.9.1	Kamil Slowikowski	https://cran.r-project.org/web/packages/ggrepel/index.html
stringr v1.4.0	tidyverse	https://stringr.tidyverse.org/index.html
dplyr v1.0.7	tidyverse	https://dplyr.tidyverse.org/index.html

(*Continued on next page*)

Continued

REAGENT or RESOURCE	SOURCE	IDENTIFIER
Shiny v1.7.2	Rstudio Team	https://shiny.rstudio.com/
shinymanager v1.0.400	Benoit Thieurmel, Victor Perrier	https://datastorm-open.github.io/shinymanager/
shinydashboard v0.7.2	Rstudio Team	https://rstudio.github.io/shinydashboard/
dashboardthemes v1.1.6		https://github.com/nik01010/dashboardthemes
DT v0.25	Rstudio Team	https://rstudio.github.io/DT/
biomaRt v2.48.3	Ensembl	https://bioconductor.org/packages/release/bioc/html/biomaRt.html
STAR Aligner	Alex Dobin	https://github.com/alexdobin/STAR
HTSeq	HTSeq Team	https://htseq.readthedocs.io/en/master/
edgeR v3.34.0	Bioconductor	https://bioconductor.org/packages/release/bioc/html/edgeR.html
Other		
Chondrocyte Maturation Screen Web App	This paper	chondrocyte.shinyapps.io/Live
Data from GWAS of Height		PMID: 20881960, 25282103, 30124842, 36224396
Data from GWAS of Alzheimer's and Insomnia		PMID: 30617256, 30804565
Mouse Genome Informatics	Jackson Laboratories	https://www.informatics.jax.org/
Online Mendelian Inheritance in Man (OMIM)	Johns Hopkins University	https://www.omim.org/
Human Phenotype Ontology (HPO)	Jackson Laboratories	https://hpo.jax.org/app/

RESOURCE AVAILABILITY

Lead contact

Further information and requests for resources and reagents should be directed to and will be fulfilled by the lead contact, Nora E. Renthal (nora.renthal@childrens.harvard.edu).

Materials availability

Plasmids utilized in this study, including the pooled sgRNA library, have been previously deposited by the Broad Institute at Addgene. Catalog numbers are listed in the key resources table.

Data and code availability

- Sequencing data generated in this study have been deposited at GEO and SRA and are publicly available as of the date of publication. Accession numbers are listed in the key resources table.
- This paper does not report original code.
- Any additional information required to reanalyze the data reported in this paper is available from the lead contact upon request.

EXPERIMENTAL MODEL AND SUBJECT DETAILS

Cell culture

A growth plate like chondrocyte (GPLC) cell line, derived and v-myc immortalized as published, was obtained as a gift from Dr. Vicki Rosen, Harvard School of Dental Medicine.[14,15] Immature GPLCs were maintained in DMEM/F12 (Gibco, Grand Island, NY, USA) with 10% FBS (Gibco), 100 U/mL penicillin, and 100 mg/mL streptomycin sulfate (Life Technologies, Inc., Grand Island, NY, USA), at 37°C with 5% CO_2. To induce chondrocyte maturation, cells were plated at high density in chondrogenic media (standard media as above, with the addition of 50 ug/mL ascorbate (Sigma-Aldrich) and 1x insulin-transferrin-selenium (ThermoFisher). For GPLC standardization, cells were plated at 80% density in standard media (day 0), changing to chondrogenic media 24 hours later (day 1), and harvested at different timepoints thereafter.

METHOD DETAILS

Genome-wide CRISPR-Cas9 knockout library generation

A stable Cas9-expressing GPLC cell line (Cas9-GPLC) was generated by lentiviral transduction of Cas9 coding sequence (pLX_311Cas9v2, Broad Institute). Transduced cells were selected in 32 ug/mL blastacidin for 7 days (Invitrogen). The activity of Cas9 was confirmed at 75% by flow cytometry for GFP+ following transduction of a GFP-targeting sgRNA (Figure S1C).

To ensure at the onset of all screens that cells were equally immature, populations of Cas9-GPLC chondrocytes were FACS-sorted for CD-200 negativity (BioLegend #123809). Cells were then cultured at equal plating density and passage number to achieve a supply of >200 million undifferentiated Cas9-GPLCs for use in generation of a genome-wide pooled KO library. Murine Brie CRISPR knockout pooled library was obtained from the Broad Institute Genetic Perturbation Platform. Cas9-GPLCs were transduced in an undifferentiated state at 20% confluence with lentivirus containing CP0044 Mouse Brie CRISPR Knockout Pooled Library, a library of 79,634 unique barcoded lentiviral guides to knock out each of 19,908 murine genes in replicate (4 unique guides/gene, Broad #73633). Cas9-GPLCs were infected at a low MOI (<0.3) to ensure effective barcoding of individual cells.[12] After 48 hours, cells were selected in DMEM/F12 10% FBS, 100 U/mL penicillin, 100 mg/mL streptomycin sulfate, with 8 ug/mL puromycin dihydrochloride (Sigma-Aldrich P9620). After 72 hours of selection, cells were collected for use in differentiation assays. 800 million KO cells were generated for primary maturation assays, investigating two time points: day 4 and day 15.

Chondrocyte maturation assay

A representation of at least 500 KO-GPLCs per guide[66] were plated in monolayer at 80% confluency in standard media (day -1), changing to chondrogenic media 24 hours later (day 0), and harvested for CD200 FACS at day 4 or day 15. A total of 600 million KO-GPLCs were assayed (300 million per timepoint), collected in 3 replicate batches of 100 million cells. Chondrogenic media was changed every 3 days until cell harvest.

FACS sorting

Cells were trypsinized, pooled, spun down, and filtered through a 40 μM cell strainer. They were then spun down and resuspended at 1.0 x 10^7 cells/mL in PBS with 1% FBS (Gibco). Cells were incubated with Mouse Seroblock FcR (Biorad FCR4G8) for 10 minutes, followed by APC anti-mouse CD200 (BioLegend 123809) for 30 minutes. Two subsequent washes and spins were performed in PBS with 1% FBS. Cell solutions were diluted to a final concentration of 5.0 x 10^6 cells/mL. Immediately prior to FACS, DAPI (Thermo Fisher, D1306) was added to a concentration of 1 μg/mL. Flow gates to sort the top 10% CD200-expressing and bottom 10% CD200-expressing cells were established based on APC levels. Live CD200-sorted KO-GPLCs were pelleted and frozen at -80C.

RNAseq of CD200 FACS sorted wild type GPLCs

To profile gene expression of wild type GPLCs sorted by maturation, cells were plated in monolayer as described for the chondrocyte maturation assay and harvested for CD200 FACS at day 4 or day 15. Cells were sorted for CD200 according to the top/bottom 10% APC flow gates described above. Total RNA was extracted from collected cells using the Rneasy Mini Plus Kit (QIAGEN) according to manufacturer's instructions. QC was performed by NanoDrop. 70 ng of each sample was submitted to Harvard Medical School's Biopolymers Facility for KAPA mRNA HyperPrep library construction and Next Generation Sequencing. Four technical replicates were sequenced for each sample. Reads were mapped to mouse genome GRCm38 using STAR Aligner[67] and gene-based readcounts were generated using HTSeq.[68] Differential gene expression was performed in edgeR[69] after library size normalization.

DNA extraction/PCR/sequencing

gDNA was extracted from collected cells using the QIAamp DNA Blood Midi Kit (QIAGEN) according to the manufacturer's instructions with slight modifications (overnight incubation at 70°C). QC was performed by NanoDrop and quantification by Qubit dsDNA BR Kit (ThermoFisher) on a Qubit 3.0 Fluorometer. DNA was diluted and distributed evenly across a 96-well plate. PCR was performed by the Genetic Perturbation Platform at the Broad Institute using primer sets which amplify the sgRNA barcodes in the CRISPR Knockout Library. Next generation sequencing was performed on the amplified fragments to quantify amounts of each sgRNA. Read count and QC files were compiled.

Validation of primary screening targets via secondary screening

Using a guide library designed to target 162 genes of interest from the primary screen and 47 controls chosen based on their expression and lack of effect in GPLCs, with 10 guides/gene, 5000 Cas9-GPLCs per guide were plated in monolayer at 80% confluency. Screens were conducted in triplicate with 30 million cells assayed per maturation time point, i.e. 90 million cells at day 4 and 90 million cells at day 15, or a total of 180 million Cas9-GPLC KO chondrocytes screened. Cell culture, FACS sorting, DNA Extraction, PCR, sequencing, and initial data analyses were performed as described above for the primary screen.

QUANTIFICATION AND STATISTICAL ANALYSIS

Statistical analysis

Bioinformatic screening analysis

For each sgRNA barcode, sums of all read counts from each CD200-sorted cell group (top 10% CD200 and bottom 10% CD200) were generated. Log normalized reads per million for each sgRNA barcode were calculated using the following formula:

$$Log_2\ Normalized\ Reads\ Per\ Million\ =\ Log_2\left(\left(\frac{Reads\ per\ barcode\ for\ a\ condition\ (top\ 10\%\ CD200\ or\ bottom\ 10\%\ CD200)}{Total\ reads\ for\ a\ condition\ (top\ 10\%\ CD200\ or\ bottom\ 10\%\ CD200)}\right)*\left(1e^6\right)+1\right)$$

Log fold change (LFC) for each sgRNA was calculated as:

$$LFC\ =\ log\ 2\ Normalized\ (Top\ 10\%)\ -\ log\ 2\ Normalized\ (Bottom\ 10\%).$$

To assess significance of effects, gene-level LFCs were assembled from these sgRNA-level LFCs using the Broad Institute GPP Hypergeometric Distribution Tool.[70] Each gene was assigned an average LFC, and a p-value based on the ranks of sgRNA LFCs. For each volcano plot, log_2(LFC) was plotted against -log_{10}(p-value) on a gene-level basis. As a measure of consistency between replicates on a gene-level, LFCs were plotted against each other. The total least squares regression of the resulting distribution was also calculated.

Meta-analysis methods

For more robust comparison of data across different screening replicates and timepoints, a meta-analysis Z-score (day 4, day 15, Combined) was generated for each sgRNA. Using the sgRNA-level LFC data calculated above, Z-scores were calculated using the following formula, in which LFC_n is the log fold change for a sgRNA from a specific replicate or condition, μ_n is the population mean of all sgRNA-level LFCs for that group, and σ_n^2 is the population variance for that group:

$$Z_{meta}\ =\ \frac{\left(\frac{LFC_1-\mu_1}{\sigma_1^2}\right)+\left(\frac{LFC_2-\mu_2}{\sigma_2^2}\right)+\ldots}{\sqrt{\sigma_1^2+\sigma_2^2+\ldots}}$$

Gene-level Z-scores and rank-based p-values were assembled from these sgRNA-level Z-scores using the Hypergeometric Distribution Tool as shown above.

Screening quality control

To assess concordance between replicates in both the primary and secondary screens, Imm vs Mat Average Fold Change (log2) values were plotted against each other. Due to lack of a dependent variable in these comparisons, total least squares regression formulas were calculated. The slopes of these formulas were compared against y = x, the null hypothesis.

To assess overall concordance between primary and secondary screening results, Imm vs Mat Average Fold Change (log2) values were plotted against each other for KOs that appeared in both screens. Pearson's R was calculated for these comparisons using the R 'cor' function with method 'pearson' to evaluate correlation.

Since each KO was represented in the primary screen at a depth of 4 guides / gene and in the secondary screen at 10 guides / gene, we tested whether any guides or genes were lost due to lack of guide representation in either screen. In the primary screen, 161 guides had 0 read counts across any replicate at Day 4 (161/79633 = 0.20%), and 301 guides had 0 read counts across any replicate at Day 15 (301/79633 = 0.38%). From loss of these guides, only 1 gene dropped out entirely at Day 4, Snhg4, and no genes dropped out at Day 15. All guides for all genes were represented in the secondary screen prior to outlier removal.

KEGG pathway analysis

Strength of KEGG pathway association[71] was calculated as log_{10}(observed / expected), where "observed" is the number of KOs genes found by primary screening and "expected" is the number of genes expected to be annotated with this term in a random gene network of the same size. False Discovery Rate (FDR) was calculated to describe the significance of enrichment; p-values were corrected for multiple testing within each category using the Benjamini–Hochberg procedure.

Height GWAS gene prioritization analysis

Gene prioritization analysis was performed using Benchmarker,[11] which in short, is an unbiased gene prioritization strategy based on a leave-one-chromosome-out (LOCO) approach, where GWAS summary statistics from 21 chromosomes are used to prioritize genes on the withheld chromosome. Similar to the default Benchmarker settings, the top 10% of genes on the withheld chromosome with the highest method-specific prioritization score were selected as prioritized. We used summary statistics from two large GWAS of height (2018[3] and 2022[4]), and 3 gene prioritization methods (DEPICT, MAGMA v.1.07, PoPS) to prioritize genes for each GWAS.

Genes were prioritized using DEPICT by prioritizing genes outside the input loci. We used genome-wide significance as the cut-off for the 2018 height GWAS and the top 500 COJO SNPs from the 2022 height GWAS as input to the gene prioritization. The 1000 genomes European reference panel was used for DEPICT.

MAGMA does not directly perform gene prioritization, however, we conducted LOCO GSEA and subsequently prioritized genes on the withheld chromosome using the method presented by Fine et al. Gene p-values were based on the snp-wise mean model. The

1000 genomes European reference panel was used to calculated LD between SNPs. The gene-based p-values for the 2022 height GWAS was based on a meta-analysis of ancestry-specific MAGMA gene p-values using appropriate reference panels to match the GWAS population.

PoPS were run using the default (and recommended) settings using the above-described MAGMA gene p-values for the 2018 and 2022 height GWAS as input.

MAGMA Gene Set Enrichment Analysis

MAGMA (v1.07) was used to assess association between our gene-level CRISPR screening prioritization data and several height GWAS published over a 12-year period (2010: n = 183,727, 2014: n = 253,288, 2018: n = 693,529, 2022: n = 5,380,080). SNP-level height GWAS summary statistics for 2010,[1] 2014,[2] 2018[3] were obtained from the GIANT consortium data files portal (https://portals.broadinstitute.org/collaboration/giant/index.php/GIANT_consortium_data_files). Gene-level GWAS p-values were compiled using MAGMA's snp-wise mean model, with 1000 Genomes European reference data used to estimate LD between SNPs (REF), and genome build GRCh37 was used.

Gene names in our CRISPR screening data were converted from mouse to human orthologs using Ensembl build 105.[72] Corresponding Z-score absolute values for day 4, day 15, and combined meta-analyses (described earlier) were used as covariates for MAGMA's two-sided gene-set analysis association test.

Conditional analyses were performed using the same method to assess the effects of various gene properties on GWAS association. Covariates were conditioned on day 4 Z-score absolute values, day 15 Z-score absolute values, inclusion in the 162 genes selected for secondary screening, and inclusion in a list of Mendelian genes involved in height from OMIM.

Binomial gene list analysis

Two-tailed binomial test was performed, comparing the proportion of genes above a significance threshold of -log10p > 2 in our screening data with the proportion of genes above this same screening threshold in a PoPS-MAGMA-DEPICT - prioritized list of genes from two height GWAS. A significance cutoff of $-\log_{10}(\text{p-value}) > 2$ for our screening data was used, and a binomial distribution was generated based on $\frac{-log_{10}(GPLC\ KO\ p-value)\ >\ 2}{Total\ Screening\ Genes}$ and the number of genes in the prioritized gene sets. Using $\frac{-log_{10}(GPLC\ KO\ p-value)\ >\ 2}{Total\ Prioritized\ Genes}$, p-values were computed from the cumulative probability function of this distribution.

Kolmogorov-Smirnov test

One-sided Kolmogorov-Smirnov test was performed, comparing Z-score rank-based distributions of our full day 4, day 15, and meta-analyzed screening datasets with rank-based distributions composed of our prioritized 2018 and 2022 (European Only) height GWAS lists. D-statistics and p-values were computed for both sides of the test (''greater'' and ''less''), and the more significant value was reported.

LD score regression

Stratified LD Score Regression (s-LDSC) v1.0.1[73] was performed to evaluate the partitioned heritability enrichment. Genome-wide binary annotations were created from gene lists by annotating all SNPs falling within the top 5% of ranked genes as 1 and all other SNPs as 0. Analyses were performed using EUR LD scores and using genome build GRCh37. Heritability enrichment was evaluated using the baseline LD model and optionally additionally SNPs in the height GSEA intersect (binarized using the same approach described above). Tau* and Tau* SE were calculated as described in Gazal 2017 Nature Genet., using common SNP annotation standard deviations (MAF >0.05), height heritability calculated from the relevant GWAS, and model output coefficients and standard errors.

$$\tau_c^* := \frac{M_{h_g^2} \cdot sd_c}{h_g^2} \widehat{\tau}_c$$

Background barcode drift analysis

Similar to our CD-200-based maturation assay, to analyze for drift in background barcode counts, due to cell proliferation or death, KO Cas9-GPLC chondrocytes, transduced with secondary sgRNA libraries, were grown at high-density in chondrogenic media for 4 or 15 days, trypsinized and stained with DAPI prior to FACS to collect all DAPI-negative cells. DNA from KO Cas9-GPLC chondrocyte libraries at baseline (day 0), day 4, and day 15 was extracted, and underwent PCR and sequencing as described for the primary screen. LFCs for day 0 vs day 4 and day 0 vs day 15 were calculated based on barcode counts. Each gene was assigned an average LFC, and a p-value based on the ranks of sgRNA LFCs. Principal component analysis (PCA) was performed on a dataset comparing barcode count LFCs with secondary screening maturation LFCs for each timepoint. Principal component 1 (PC1) was calculated to adjust KOs affecting chondrocyte maturation for the effects of proliferation. Top 10 secondary screening hits at day 4 and 15 were re-ranked based on their new eigenvalues.

Secondary screen outlier analysis

Our secondary screening library represented each gene at a rate of 10 guides/gene. To assess and remove the effects of potentially faulty sgRNAs from our data, we performed outlier analysis. Interquartile range (IQR) was defined as the spread of a dataset (Q_3 - Q_1). If the average log fold change for a sgRNA was greater than Q_3 + (1.5 * IQR) or less than Q_1 - (1.5 * IQR), it was marked as an outlier. sgRNA outliers were then removed from the final data.

Software

R software tools

Statistical analyses, data manipulation, and graphical visualizations were performed using R Statistical Software (v4.1.0; R Core Team 2021) in Rstudio (v2022.7.1.554, Rstudio Team 2022). Visualizations were generated using ggplot2 (v3.3.5, https://ggplot2.tidyverse.org), ggrepel (v0.9.1, https://cran.r-project.org/web/packages/ggrepel/index.html), and stringr (v1.4.0, https://stringr.tidyverse.org/index.html). Data manipulation was aided by dplyr (v1.0.7, https://dplyr.tidyverse.org/index.html). Webtool built in Shiny (v1.7.2, https://shiny.rstudio.com/), using shinymanager (v1.0.400, https://datastorm-open.github.io/shinymanager/), shinydashboard (v0.7.2, https://rstudio.github.io/shinydashboard/), dashboardthemes (v1.1.6, https://github.com/nik01010/dashboardthemes), and DT (v0.25, https://rstudio.github.io/DT/). Gene name analog conversion was performed using biomaRt (v2.48.3, https://bioconductor.org/packages/release/bioc/html/biomaRt.html). RNAseq analysis was performed using STAR Aligner (https://github.com/alexdobin/STAR), HTSeq (https://htseq.readthedocs.io/en/master/), and edgeR v3.34.0 (https://bioconductor.org/packages/release/bioc/html/edgeR.html).